Published online 22 November 2018

Nucleic Acids Research, 2019, Vol. 47, No. 2 ***679–699***
doi: 10.1093/nar/gky1135

Retrograde BMP signaling activates neuronal gene expression through widespread deployment of a conserved BMP-responsive *cis*-regulatory *activation element*

Robin Vuilleumier[1,*], Tianshun Lian[1,†], Stephane Flibotte[1,†], Zaynah N. Khan[1,†], Alisa Fuchs[2,3], George Pyrowolakis[2] and Douglas W. Allan[1,*]

[1]Department of Cellular and Physiological Sciences, University of British Columbia, Vancouver, British Columbia, Canada, [2]BIOSS, Centre for Biological Signaling Studies and Institute for Biology I, Faculty of Biology, Albert-Ludwigs University of Freiburg, Freiburg, Germany and [3]Max-Planck Institute for Molecular Genetics, Berlin, Germany

Received February 19, 2018; Revised October 22, 2018; Editorial Decision October 24, 2018; Accepted October 25, 2018

ABSTRACT

Retrograde Bone Morphogenetic Protein (BMP) signaling in neurons is essential for the differentiation and synaptic function of many neuronal subtypes. BMP signaling regulates these processes via Smad transcription factor activity, yet the scope and nature of Smad-dependent gene regulation in neurons are mostly unknown. Here, we applied a computational approach to predict Smad-binding *cis*-regulatory *BMP-Activating Element*s (*BMP-AE*s) in *Drosophila*, followed by transgenic *in vivo* reporter analysis to test their neuronal subtype enhancer activity in the larval central nervous system (CNS). We identified 34 *BMP-AE*-containing genomic fragments that are responsive to BMP signaling in neurons, and showed that the embedded *BMP-AEs* are required for this activity. RNA-seq analysis identified BMP-responsive genes in the CNS and revealed that *BMP-AE*s selectively enrich near BMP-activated genes. These data suggest that functional *BMP-AE*s control nearby BMP-activated genes, which we validated experimentally. Finally, we demonstrated that the *BMP-AE* motif mediates a conserved Smad-responsive function in the *Drosophila* and vertebrate CNS. Our results provide evidence that BMP signaling controls neuronal function by directly coordinating the expression of a battery of genes through widespread deployment of a conserved Smad-responsive *cis*-regulatory motif.

INTRODUCTION

With its extraordinarily high cellular diversity that underpins its multiple functions, the central nervous system (CNS) is the most complex organ in most animals. The generation of such a high diversity of neuronal subtypes requires that they undergo unique programs of differentiation as young maturing neurons. Extensive work has shown that these programs are primarily determined by the activities of subtype-specific combinatorial codes of transcription factors acting at *cis*-regulatory regions of target genes (1–4). Considerable evidence also supports a critical contribution of retrograde signaling from target cells to neuronal differentiation and function, in mammals and *Drosophila* (5–7). However, even though such a role is long established, the networks of genes they control and the genomic enhancers they operate through remain largely undiscovered. Thus, the molecular mechanisms underlying the contribution of these retrograde signals remains undefined for the most part.

In the larval *Drosophila* ventral nerve cord (VNC), retrograde Bone Morphogenetic Protein (BMP) signaling occurs in efferent neurons (8–13). It is required by neuropeptidergic efferents for neuropeptide gene specification (10–13) and by motor neurons for synaptic growth, stability, neurotransmission and homeostasis of the neuromuscular junction (NMJ) (9,14,15). The BMP ligand Glass bottom boat (Gbb) is secreted from postsynaptic cells and from motor neurons (12,16), to bind a presynaptic BMP receptor complex of type II BMP receptor, Wishful thinking (Wit), and the type I BMP receptor kinases, Thickveins (Tkv) and Saxophone (Sax) (9,14,17). Accumulating evidence indicates that after BMP activation, these receptors are endocytosed for retrograde transport to the soma (18–20). BMP recep-

*To whom correspondence should be addressed. Tel: +1 604 827 5960; Fax: +1 604 822 2316; Email: doug.allan@ubc.ca
Correspondence may also be addressed to Robin Vuilleumier. Email: robvuill@mail.ubc.ca
† The authors wish it to be known that, in their opinion, authors two to four should be regarded as Joint Second Authors.

tor kinase activity phosphorylates the cytoplasmic R-Smad, Mother against decapentaplegic (Mad), which binds the co-Smad, Medea, to form a pMad/Medea (pSmad) complex that accumulates in the nucleus, where it regulates gene expression (10,12,17,21). Motor neuron and neuropeptidergic cell phenotypes characterized for *gbb, wit*, *tkv* and *sax* mutants are largely phenocopied in *Mad* and *Med* mutants and upon overexpression of DNA-binding defective Mad (9,17,21,22). Thus, BMP signaling via pMad/Medea-responsive gene regulation appears to play a critical role in motor neuron and neuropeptidergic cell function.

Numerous genes are regulated by retrograde BMP signaling in *Drosophila* efferent neurons. In neuropeptidergic efferents, this includes the activation of subtype-specific neuropeptides in FMRFa-Tv4, CCAP and Ilp7 neuropeptidergic cells (10,11,13). The GPI-anchored Ly6 gene, *target of wit (twit)* (23), and the guanine nucleotide exchange factor, *trio* (24), are upregulated in motor neurons by BMP signaling, and act as effectors of BMP function at the NMJ. However, neither *twit* nor *trio* mutants fully phenocopied *wit* mutants, and restoration of these genes in *wit* mutants only partially rescued the *wit* phenotype; implicating additional undefined genes as BMP effectors. A microarray study reported the differential expression of 101 genes in the late larval CNS of controls and *wit* mutants, which included *twit* as well as two other confirmed *wit*-responsive genes, *Pburs* and *FMRFa* (25). These additional genes represent candidate BMP effector genes, although they remain unverified as direct targets of pMad/Medea complexes; only in the cases of *FMRFamide* (*FMRFa*) and *trio* has such evidence been provided (24,26). Thus, we still know very little about the direct coordinated gene regulatory processes controlled by BMP signaling and pMad/Medea transcriptional activity that underlies neuronal differentiation, plasticity and synaptic function.

Numerous *cis*-regulatory motifs that are bound by pMad/Medea complexes have been described in *Drosophila* that mostly converge around *GC*-rich binding motifs (27–36). From these studies, two motifs have had their precise sequence requirements rigorously characterized *in vitro* and *in vivo* (33–35) and mediate *cis*-regulatory activity in a number of developmental contexts. These include a *silencer element* termed the *BMP-SE*, which mediates repression of *brinker* and other genes (35,37–42), and also an *activating element* (*BMP-AE*) that mediates activation of *daughters against decapentaplegic* (*dad*) and the enhancer activity for numerous genomic regions throughout fly development (34). The 15 bp consensus sequence of the *BMP-AE* comprises two distinct binding sites optimally separated by a 5-nucleotides linker, a *GGCGCC* site bound by two pMad, and a Medea-bound *GNCV* site (*V* = any nucleotide except *T*) (34) (Figure 1A). Although a function for the *BMP-AE* has not been demonstrated in the nervous system, we postulated that it may serve as a platform for retrograde BMP-activated gene transcription in neurons.

The high cellular diversity of the larval *Drosophila* nervous system and the neuron subtype-specific expression of most defined BMP-responsive genes makes genomic approaches to identifying their *cis*-regulatory elements challenging. However, the sequence complexity of the *BMP-AE* allows for a computational approach to predict BMP-responsive enhancers and genes in neurons. Identification of functional *cis*-regulatory elements has been successfully performed using bioinformatics algorithms that scan the genome for conserved instances of transcription factor binding site sequences (43–47). Here, we combined the identification of highly conserved *BMP-AE* sequences near neuronally expressed genes with transgenic enhancer activity analysis *in vivo* to discover a co-regulated battery of 34 *wit* and pMad/Medea-responsive genomic fragments that are active in efferent (motor neurons and/or neuropeptide expressing) neurons. RNA-seq expression profiling of *wit* mutant VNCs revealed that functionally-validated *BMP-AEs* are enriched to BMP-activated genes and that most of them locate within 20 kb of the transcription start site of a BMP-activated gene. We further demonstrated a direct regulatory relationship between *BMP-AE*s and BMP-activated genes by functional testing of the three *BMP-AE*s within the *twit* gene locus. Finally, we showed that the *BMP-AE* motif has a conserved function in the nervous system by chick neural tube electroporation, and by the demonstration that a *BMP-AE* taken from the *Xenopus bambi* BMP-responsive enhancer functionally replaced a fly *BMP-AE in vivo*.

Our results show that the *BMP-AE* motif is a widely used, conserved pMad/Medea-responsive element that mediates co-regulation of a battery of BMP-activated genes in *Drosophila* efferent neurons. We further demonstrate the utility of such sequences in computational searches for BMP-responsive genes and enhancers in the nervous system, and provide a framework for analysis of the transcriptional mechanisms underlying synaptic growth and neurotransmission.

MATERIALS AND METHODS

BMP-AE identification and prioritization

Using merMER *(*http://www.insilicolabs.com/experiment/index.php*)*, we identified 775 occurrences matching the *BMP-AE* sequence (*GGCGCCANNNNGNCV*) in the *D. melanogaster* genome (48). With the assistance of the Stark group, these were filtered by the controlled Branch Length Score (BLS) method to evaluate phylogenetic conservation over 12 *Drosophila* species and assigned a motif confidence score based on the relative conservation of the *BMP-AE* and control motifs (43,44) (Supplementary Figure S2, Supplementary Table S1). Of these, we selected the following *BMP-AE*s only if they were located in noncoding DNA within 12kb of the locus of a gene expressed in the late larval central nervous system: (A) All *BMP-AE*s with a motif confidence of 1 or 0.9 (where 0 is lowest confidence and 1 is highest confidence) were analyzed. (B) All *BMP-AE*s with a motif confidence of 0.8 were analyzed, if 'paired' with another *BMP-AE* of motif confidence $\geq$0.9 within 12 kb of the same annotated gene locus. (C) All *BMP-AE*s with a motif confidence of 0.8 were analyzed, if more than two were found within 12kb of the same annotated gene locus. (D) An additional two unpaired *BMP-AE*s with a motif confidence of 0.8 were also analyzed. This filtering led to the prediction of 62 *BMP-AE* candidates (43 intronic, 3 UTR, 16 intergenic) located near ~46 neuronally-expressed genes. Release 3 of the *Drosophila melanogaster* reference genome assembly (Dm3) was used for this initial computational anal-

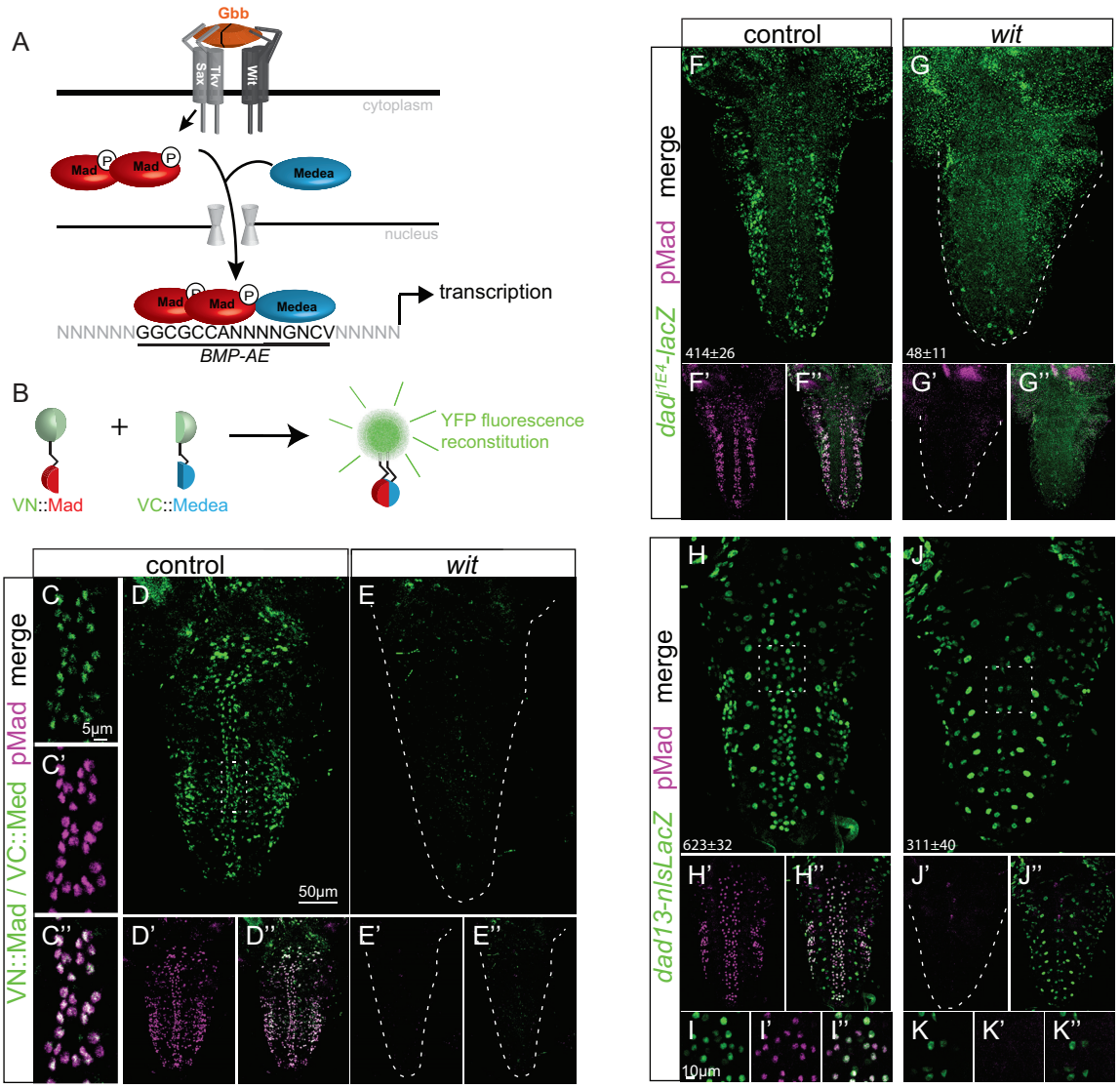

Figure 1. A canonical BMP signaling pathway acts in neurons. (**A**) Schematic representation of the canonical fly BMP signaling pathway and binding of pMad and Medea to *cis*-regulatory *BMP-AE* sequences. (**B**) Schematic of the BiFC method. Mad and Medea are fused to two split non-fluorescent fragments of Venus YFP. Upon co-expression of both constructs, direct interaction between VN::Mad and VC::Medea allows for reconstitution of fluorescence. (**C–E”**) Bimolecular Venus YFP fluorescence is specific to nuclei with BMP activity in L3 VNCs, as revealed by overlap with immunoreactivity to pMad in control genotypes (**C–D”**), and its absence in *wit* mutants (**E–E”**). (**F–K”**) β-galactosidase expression of the *dad* enhancer trap dad^{j1E4} (**F–G”**) and the *dad13-nlsLacZ* reporter construct (**H–K”**), shown with pMad co-immunostaining in controls (**F, H-I”**) and *wit* mutants (**G, J–K”**). (**I–I”, K–K”**) Close up of immunoreactivity at the dorsal midline taken from the region of the square dotted box in H and J, respectively. The mean±SEM number of nuclei per VNC that express the reporter is indicated at the bottom of each images. Reporter activity of both dad^{j1E4} and *dad13-nlsLacZ* was significantly reduced in *wit* mutants as dad^{j1E4}: $P = 0.0022$ and *dad13-nlsLacZ*: $P = 0.0012$ (two-sided Wilcoxon rank-sum test). At least 5 VNCs were analyzed for each genotype. Genotypes: (C, D): *pUbi-VC-Medea/+; pUbi-VN-Mad,* wit^{A12}*/+*. (**E**): *pUbi-VC-Medea/+; pUbi-VN-Mad,* wit^{A12}/wit^{B11}. (F) dad^{j1E4}, $wit^{A12}/+$. (G) dad^{j1E4}, wit^{A12}/wit^{B11}. (H, I) *dad13-nlsLacZ/+;* $wit^{B11}/+$. (J, K) *dad13-nlsLacZ/+;* wit^{A12}/wit^{B11}.

ysis (49). Coordinates for *BMP-AE* were later converted to Release 6 (Dm6) coordinates for matching their proximity to BMP-regulated genes, as determined by RNA-seq (see below). Determination of neuronally-expressed genes was taken from late third instar CNS gene expression data available, according to the FlyAtlas microarray database (50) or RNA-seq data available from the modENCODE consortium (51) or the Knoblich group (52).

Fly strains and chick embryos

Flies were reared on standard medium at 25°C, 70% humidity. *VN::Mad* and *VC::Medea* (53), *dad13-lacZ* (34), *UAS-dad* and dad^{j1E4}*-lacZ* (54), *UAS-*tkv^{DN} (55), wit^{A12} and wit^{B11} (9), *elav-GeneSwitch-GAL4* (56), $twit^{160}$ (23), *Mi{MIC}*$twit^{MI06552}$ (57) were provided by the Bloomington *Drosophila* Stock Center. w^{1118} was used as control if not otherwise stated. Eggs from White-Leghorn chickens (*Gallus gallus*) were obtained from University of Alberta,

Canada, incubated at 39°C and staged according to Hamburger and Hamilton (HH) (58).

Drosophila DNA constructs, transgenic flies and neuronal BMP signaling knock down

A list of all primers used in this study can be found in Supplementary Table S1. To generate reporter constructs, approximately 2 kb genomic DNA fragments were amplified by PCR and cloned into the pCR8/GW/TOPO entry vector by TA cloning (Invitrogen) or the pJet1.2/blunt vector (Thermo Fisher). The 2 kb genomic fragment size is in line with other studies performing large scale enhancer identification in *Drosophila* (34,59,60), and is a good compromise between cloning efficiency of large DNA fragments and reducing the chance of excluding important enhancer elements on either side of a putative *BMP-AE*. Genomic fragments were cloned into the pattBGWhZn destination vector (61) by Gateway cloning (Invitrogen) or into the EcoRI and BamHI sites of the pStingerattBDsRednls. For the *twit* genomic locus, a 6.1 kb DNA fragment was amplified from the BAC CH322-97H12 (P[acman] Resources) by PCR and cloned into the KpnI and HpaI sites of the pStdTomatoattB. Mutagenesis was performed by SOE-PCR, using primers designed to introduce the specific point mutations. All constructs were verified by sequencing.

For fly transgenesis, constructs were inserted via PhiC31 mediated site-specific integration (62) at either insertion site attP40 (25C6) or VK37 (22A3) on chromosome 2 or at attP2 (68A4) on chromosome 3 by Genetics Services Inc. (MA, USA) and Rainbow Transgenics Flies Inc. (CA, USA). Transgenic knock-down of BMP signaling in neurons was carried out using *elav-GeneSwitch-GAL4* (56). To activate GeneSwitch-GAL4 from embryonic stages onwards, mothers were fed with yeast paste containing 10–12 μg/ml of RU486 (Mifepristone) for 2 days before being crossed with males. Larvae were then fed with standard food containing 8–10 μg/ml of RU486 until dissection.

Immunofluorescence, *in situ* hybridization and microscopy

Standard procedures were used for immunostaining of *Drosophila* VNCs and vibratome sections of chicken embryos. Primary antibodies were chicken anti-βgal (1:1000; ab9361) and chicken anti-GFP (1:1000, ab13970) (Abcam); mouse anti-βgal (40-1a, 1:5), mouse anti-Elav (9F8A9, 1:10) and mouse anti-Pax7 (1:5–10) (Developmental Studies Hybridoma Bank, University of Iowa, USA); guinea pig anti-Dimmed (1:500; a gift from Dr. S. Thor); rabbit anti-pSmad1/5 (1:100; 41D10; Cell Signaling Technology). Secondary antibodies were donkey anti-Mouse, anti-Chicken, anti-Rabbit, anti-Guinea Pig conjugated to FITC, DyLight 488, Cy3, Cy5 and Alexa 647 (1:500–1:5000; Jackson ImmunoResearch). Images of experimental groups were captured the same day using the same settings with an Olympus FV1000 confocal microscope.

For *in situ* hybridization of *twit*, the cDNA clone LD40063 was obtained from *Drosophila* Genomics Resource Center (DGRC, University of Indiana, USA) and was used to synthesize a 1141 bases Dig-labeled RNA probe by *in vitro* transcription using the DIG RNA labeling kit (Roche). Whole third instar larvae carcasses flipped inside out were fixed in 4.2% formaldehyde for 40 min (10 min. on ice and 30 min. at RT) and washed with RNase-free PBS. After methanol storage for at least 12 h at −20°C, they were rehydrated in PBS Tween 20 (0.1%) (PBSTw) and pre-hybridized in pre-hybridization buffer (50% formamide, 4× SSC, 0.01% Tween 20, pH 6) for 1 h at 55°C. The *twit* Dig-labeled RNA probe was diluted (1 ng/μl) in hybridization buffer (50% formamide, 4× SSC, 0.01% Tween-20, 5% dextran sulfate, pH 6), heated at 80°C for 3 min and chilled on ice cold water for 5 min. The riboprobe was added to the samples and hybridization was carried out for 24 h at 55°C in a Bambino Hybridization Oven (Boekel Scientific). After washing the samples five times in hybridization washing buffer (50% formamide, 2× SSC, 0.01% Tween 20, pH 6) with the last wash overnight at 55°C, they were washed four times in PBSTw and blocked for 1 h at RT in PBSTw with 5% normal donkey serum. Following overnight incubation of the samples with anti-Digoxygenin antibodies (1:2000, Roche) diluted in the blocking solution at 4°C, they were washed six times with PBSTw and two times with the alkaline phosphatase buffer (100 mM Tris–HCl pH 9.5, 50 mM $MgCl_2$, 100 mM NaCl, 0.2% Tween 20) before incubation in NBT/BCIP staining solution (Roche).

Quantification of reporter expression in the ventral nerve cord

To compare reporter expression in control and *wit* mutant VNCs, we examined tissues fluorescent for nlsDsRed or immunofluorescent for nuclear localized βgal, anti-Elav (neuronal nuclei) and anti-pMad (nuclei of BMP signaling activated cells). In all cases, five or more VNC were dissected and imaged for each genotype. All tissues to be compared were processed in the same tube with the same reagents, mounted on the same slide and also imaged and analyzed in identical ways. To quantitate reporter activity, we used Bitplane:Imaris v9.2 software (in Spots Mode) to identify reporter-positive nuclei in the VNC (excluding the brain lobes), and in controls we additionally filtered these for pMad co-immunoreactivity (by median intensity thresholding). As there was no pMad immunoreactivity in *wit* mutants, we counted the number of reporter-positive nuclei in this genotype, which was compared to control numbers. We also compared the percentage loss of reporter expression in *wit* mutants, to the percentage of reporter-positive nuclei that were pMad-co-immunoreactive in controls. Imaris settings were established independently for each set of reporters, in order to provide optimal 'spot' marking of verifiable reporter and pMad co-immunoreactive nuclei, with minimal background fluorescence spot marking. Each image was further subtracted, manually, for spots that erroneously labelled background fluorescence.

For intensity measurements of reporter fluorescence in dorsal midline motor neurons, fluorescent intensity of individual motor neuron nuclei (Elav-positive) was measured in ImageJ (US National Institutes of Health). Mean pixel intensity for each motor neuron was measured from summed Z-projections to measure the total mean fluorescence intensity for each VNC. For each VNC, we subtracted the mean background fluorescence intensity, which was measured from 10 adjacent Elav-negative locations, using the

same circular area as for Elav-positive nuclei. At least 5 VNCs with at least 40 motor neurons per VNC were analyzed. Each data point representing the mean of total reporter fluorescence intensity for a genotype was then expressed as a percentage of the mean of the control group.

Statistical analysis and graphing were performed using the online tool at https://ccb-compute2.cs.uni-saarland.de/wtest/ (63) and MS Excel, respectively. All multiple comparisons were carried out using the two-sided Wilcoxon rank-sum test. Differences between genotypes were considered significant when $P < 0.05$. Data are presented as mean ± standard error of the mean (SEM).

Electrophoretic mobility shift assay (EMSA)

FLAG::Mad, Myc::Medea, and/or Tkv^{QD} cDNA sequences were derived from previously described vectors (33,37) (a gift from Dr A. Laughon) and subcloned into a pAc5.1/V5-His vector backbone (ThermoFisher). For EMSA, 3×10^6 *Drosophila* S2 cells in 2 ml medium were co-transfected with 2.4 μg of total expression plasmids consisting of 800 ng Tkv^{QD}, 800 ng FLAG::Mad and 800 ng Myc::Medea and/or empty pAc5.1 using the XtremeGENE HD transfection kit (Roche). Forty eight hours following transfection, cells were harvested, washed with PBS and lysed for 15 min in 90 μl ice-cold lysis buffer containing 100 mM Tris–HCl pH 7.6, 0.5% Tween-20, 1 mM DTT and 1× Roche cOmplete ULTRA EDTA-free Protease inhibitor cocktail. The lysate was cleared by centrifugation and stored at −80°C until use. Oligonucleotides synthesized and labelled with IRDye700 by Integrated DNA Technologies (IDT) were annealed to generate probes. Binding reactions were carried out in 20 μl of reaction buffer containing 25 mM Tris pH 7.5, 35 mM KCl, 80 mM NaCl, 3.5 mM DTT, 5 mM $MgCl_2$, 0.25% Tween 20, 1 μg poly dIdC, 10% glycerol and 1× cOmplete ULTRA EDTA-free Protease inhibitor cocktail (Roche). DNA and protein binding was performed by incubating 20 μg of lysate protein with 1 μl of 50nM IRDye700-labeled probe for 30 min at room temperature. The reactions were resolved by non-denaturing 4% polyacrylamide gel electrophoresis and analysed using a Licor Odyssey Imager system (Lincoln, NE).

Chicken spinal cord electroporation

Eight repeat concatemers of the wildtype and mad site mutated *dad13 BMP-AE* were obtained using ultramers (IDT) that were cloned into the Acc65I and BglII sites of the *ptk-EGFP* (64) (a gift from Dr A. Kania) to generate *BMP-AE8x-EGFP* and *BMP-AE*$8x^{\Delta mad}$*-EGFP* plasmids. Sequences can be found in Supplementary Table S1.

The *BMP-AE8x-EGFP* and *BMP-AE*$8x^{\Delta mad}$*-EGFP* plasmids (390–500 ng/μl) were co-electroporated with a control *pCAGGS-IRES-H2B-RFP* plasmid (130–500 ng/μl) (a gift from Dr E. Marti) to verify electroporation efficiency or a *pCAGGS-SmadSD-IRES-H2B-RFP* plasmid (a gift from Dr E. Marti) to increase BMP signaling. Plasmid DNA diluted in water and 0.05% Fast Green (Sigma) were microinjected into the lumen of neural tubes of Hamburger Hamilton (HH) stage 14 embryos. Following microinjection of plasmid DNA using a Picospritzer® 2 (General Valve Corporation) microinjector, tungsten electrodes (2 mm) were placed at the lumbar spinal cord level with a spacing of 4 mm between the anode and the cathode and a current was applied using an Electro Square Porator ECM 830 (BTX) electroporator (settings: 30 V, 5 pulses of 50 ms wide in a 1 s interval). Following electroporation, Tyrode's saline solution supplemented with 10% Penicillin and Streptomycin and 1% Fungizone was added on top of the embryos. After sealing the egg shell, embryos were further incubated at 39°C for 24 or 48 h before harvesting.

RNA isolation, sequencing, analysis and enrichment of *BMP-AE* motifs near BMP-regulated genes

To minimize variation between experimental groups, first instar larvae were transferred to fresh vials at a density of 80 larvae/vial until the desired stage. Whole CNS from $w^{1118};;wit^{A12}/+$ and $w^{1118};;wit^{A12}/wit^{B11}$ wandering third instar female larvae were dissected free of all other tissues in ice cold PBS and brain lobes were removed to isolate VNCs. VNCs were placed in RNAlater (Ambion, ThermoFisher) and stored at −20°C until the day of RNA extraction. Four independent biological samples of 25 VNCs each were prepared for both genotypes. Total RNA was extracted using RNAzol® RT (Millipore, Sigma) following the manufacturer's protocol, except that the RNA pellet was washed four times with 75% ethanol before solubilization in RNase-free water. Total RNA quality and concentration was assessed using an Agilent 2100 Bioanalyzer (Agilent). Libraries for RNA-seq were generated using the Illumina Neoprep System and sequenced using the Illumina Nextseq500 (Illumina), collecting a total of 24–35 million read pairs (2 × 80 nucleotides long).

In a preliminary analysis, multiple pipelines have been applied. Briefly, for the alignment stage we used STAR (65) and HISAT2 (66) and the pseudo aligners kallisto (67) and Salmon (68). Quantification was performed directly with STAR, kallisto and Salmon or with RSEM (69) and StringTie (66) for the pipelines producing real alignments. In all cases the reference transcriptome was from release 6 of the *Drosophila melanogaster* reference genome assembly (Dm6) (70). The alignment rate was consistent at 93–94% for all the samples. In-house Perl scripts were used to sum the read counts at the transcript level for each gene and create matrices comprising the read counts for all of the genes for all of the samples. Differential expression analysis was then performed on the data from those matrices using the R package DESeq2 (71), edgeR (72), sleuth (73) and Ballgown (66). Each sample was assessed using the quality-control software RSeQC and the PtR script from the trinity suite (74). No potential outliers were detected when clustering the samples and therefore all the samples were kept for the differential expression analysis. The output for each pipeline is a list of genes ranked by the *P*-value for differential expression after correction for multiple testing with a significance cutoff set at $P<0.05$. A combined list was obtained

by ranking the genes according to their median rank from the various analysis pipelines and only genes achieving the significance cutoff in at least half the pipelines were considered as significantly differentially expressed. Genes with differential expression not going in a consistent direction between pipelines were eliminated from that combined list of significant genes. The kallisto-DESeq2 pipeline gave results close to the combined list and for sake of simplicity only the numerical output from that pipeline is reported in the current work. Differential expression was determined by $\log_2$ fold change between control and *wit* mutant gene values. The display panel for differential expression shown in Figure 4A and Supplementary Figure S11 was made in R using the ggplot2 package (75).

To test for enrichment of *wit*-responsive genes to *BMP-AE*s or *bicoid*-responsive fragments (Figure 4B), we mapped the location of all *wit*-responsive genes identified by RNA-seq analysis, with the 26 bcd-responsive fragments as controls (8 of the 34 *bicoid*-responsive fragments listed in (76) had to be removed due to close proximity to one of the *BMP-AE* tested herein) and the 59 *BMP-AE* motifs contained within the 56 genomic fragments for which we could determine *wit*-responsiveness. Note that three *BMP-AE*s embedded into two genomic fragments, *Van10* and *Van19*, were excluded because we could not determine whether these were *wit*-responsive. We then counted the number of genomic loci that contain at least one *wit*-responsive gene located within a given distance of a Bcd-responsive fragment or *BMP-AE* motif within *wit*-responsive and *wit*-non responsive fragments. This approach allowed us to perform statistical analysis that avoids re-counting of the same gene(s) multiple times.

To more selectively test whether *BMP-AE*s in *wit*-responsive fragments were more likely to be directly adjacent to a *wit*-responsive gene, with no intervening *wit*-non responsive gene, we repeated the above enrichment analysis, but only considered adjacent motifs. For this analysis, we were able to separate the genomic locus 2L:8324753 into two distinct loci, due to the presence of an intervening *wit*-non-responsive gene between a pair of *BMP-AE*s and their adjacent *wit*-responsive gene. This increased the total number of loci tested to 26 for *BMP-AE* in *wit*-responsive fragments.

Statistical significance of the enrichment of *BMP-AE* and Bcd-responsive genomic fragments near BMP-dependent genes was calculated using Pearson's Chi square test for count data in R (function chisq.test) with continuity correction without correcting for multiple testing (77).

BMP-AE motif sequence enrichment calculation

The Two Sample Logo software (78) available at http://www.twosamplelogo.org/ was used to calculate and visualize the sequence difference between the 37 *BMP-AE* motifs embedded into the *wit*-responsive fragments and the 22 *BMP-AE* motifs within the *wit*-non responsive fragments as well as the 10 *BMP-AE* motifs within *tkv*-responsive fragments (34). Statistical enrichment was calculated using Student's t-test with a significance cutoff of $P < 0.05$.

RESULTS

Canonical BMP signaling acts through *BMP-activating elements* (*BMP-AE*) in neurons

Efferent neurons of the VNC accumulate nuclear phosphorylated Mad (pMad) in response to synaptic Gbb (Figure 1A). While pMad is assumed to associate with Medea to regulate transcription in neurons, this had yet to be explicitly demonstrated. To test this, we examined pMad and Medea physical interaction by bimolecular fluorescent complementation (BiFC) of split Venus yellow fluorescent protein fragments, VN and VC (53,79–82) (Figure 1B). We ubiquitously expressed VN::Mad and VC::Medea fusion proteins and examined BiFC in the VNC. Expression of either VN::Mad or VC::Medea alone did not report any fluorescence (not shown), but co-expression of VN::Mad and VC::Medea led to strong fluorescence within the nuclei of BMP-activated neurons (Figure 1C and D). We examined BiFC in *wit* mutants that have a loss of neuronal BMP signaling (9,14), and observed an absence of fluorescence in the VNC (Figure 1E). Thus, BMP activation in neurons results in the formation of pMad/Medea complexes in the cytoplasm, followed by their accumulation in nuclei.

In vivo and *in vitro* studies have shown that pMad/Medea complexes act at *cis*-regulatory sequences, termed *BMP-activating elements* (*BMP-AE*s), to activate the expression of *dad*, an inhibitory Smad, and a number of BMP-responsive genomic fragments that are active in the embryonic dorsal epidermis and larval wing imaginal disc (Figure 1A) (34). To obtain evidence for *BMP-AE* activity in neurons, we examined whether *BMP-AE*-dependent *dad* expression occurs in the VNC. First, using a faithful *lacZ* enhancer trap reporter for *dad* (dad^{j1E4}) (54), we found that *dad* was expressed in 414 ± 26 nuclei of the VNC ($n = 6$), and that 321 ± 19 (or 78%) of those nuclei were co-immunoreactive for pMad. Our counts indicate that there are approximately 742±20 pMad-positive nuclei in the VNC ($n = 14$), therefore the *dad* reporter is expressed in approximately 43% of pMad-positive nuclei. In *wit* mutants, reporter expression fell to 48 ± 11 nuclei ($n = 6$; $P = 0.0022$) (Figure 1F and G). This 88% loss of reporter expression correlates with the approximate 78% expression of the reporter in pMad co-immunoreactive nuclei, suggesting that reporter expression is largely lost from nuclei that are pMad-positive in controls. Next, to test a role for *BMP-AE*s in neuronal *dad* expression, we examined expression of the *dad13-nlsLacZ* transgenic reporter, which reports the activity of a 520 bp enhancer of *dad* mediated by a single *BMP-AE* (34). In the VNC, *dad13-nlsLacZ* was expressed more broadly than the dad^{j1E4} reporter, in 623±32 nuclei of which 486±13 (79%) nuclei were pMad-positive ($n = 7$). This represents approximately 65% of all pMad-positive nuclei. Expression in pMad-negative nuclei included glia, as evidenced by their lack of Elav co-immunoreactivity (Figure 1H-K, Supplementary Figure S1). In *wit* mutants, *dad13-nlsLacZ* reporter activity was reduced by 50% to 311 ± 40 nuclei ($n = 6$; $P = 0.0012$). This 50% loss of reporter expression was substantially less than the approximate 79% expression of the reporter in pMad co-immunoreactive nuclei, suggesting that in *wit* mutants the reporter is lost in

most but not all nuclei that are pMad-positive in controls. Comparison of reporter expression in Elav-immunoreactive nuclei in the dorsal VNC of controls and mutants indicated that reporter expression was commonly retained in most glia but also in a subset of neurons (Supplementary Figure S1). Thus, we find that these *dad* reporters exhibit *wit*-responsive activity in neurons that are pMad-positive.

Identification of 34 *wit*-responsive genomic fragments in neurons

We wished to test whether the *BMP-AE* motif plays a widespread role as a *cis*-regulatory element that can be used *in silico* to efficiently predict pMad/Medea-responsive enhancers near BMP-responsive genes in neurons. Such a method offers the advantage that it can be performed regardless of neuronal subtype gene expression, whereas genomics approaches to identify pMad-bound genomic enhancers in the *Drosophila* CNS are challenging due to the relative low number of pMad-positive nuclei, the high cell subtype diversity of pMad-positive motor and neuropeptidergic efferent neuronal populations (83,84), and the neuronal subtype diversity of known BMP-dependent genes (10,11,13,23,24).

We identified all *BMP-AE* motifs in the *D. melanogaster* genome using merMer (48). These were filtered for high conservation using the Branch Length Score to motif confidence method (Supplementary Figure S2) (43,44) and for proximity to genes expressed in the larval nervous system, from available databases (50–52). This led to our prioritization of 62 *BMP-AE*s (see Materials and Methods and Supplementary Table S1 for details). To test the *in vivo* activity of these *BMP-AE*s, 58 genomic DNA fragments (of ∼2kb) containing one or more of the 62 *BMP-AE*s were cloned in front of *lacZ* or *DsRed* reporters, both with a nuclear location signal (*nlsLacZ* or *nlsDsRed*). These genomic fragment reporters were placed into *attB* transgenic vectors for integration into the genome using phiC31-integrase (62) (see Materials and Methods and Supplementary Table S1).

We examined reporter activity driven from these genomic fragments in the VNC of wandering third instar larvae. Out of the 58 reporters, 13 showed no expression in the VNC, while 45 exhibited robust reporter activity in the VNC (Supplementary Table S1). Of these active reporters, 42 exhibited expression in subsets of pMad-positive cells in the VNC (which at this developmental stage comprises efferent neurons, e.g. motor and/or neuropeptidergic neurons) (8–11,13), and in certain cases also pMad-negative glia and neurons (Figure 1H-K, Supplementary Figures S1, S3, S4, S5). We tested the BMP-responsiveness of these reporters by placing all 42 into a *wit* mutant background. Out of those 42 reporters, 32 showed a partial to total loss of reporter expression, and 8 reporters showed no change (Figures 1H–K, 2, Supplementary Figure S6, Supplementary Table S1). For 2 reporters (*Van10* and *Van19*), we were unable to unambiguously determine if there was any *wit*-responsive activity, because they were expressed in dense clusters of pMad-positive and pMad-negative cells which we could not discriminate in *wit* mutants (due to the loss of pMad as a marker to distinguish these cells) (Supplementary Table S1).

For *wit*-responsive reporters, we wished to test if the reporter was preferentially lost in cells that are pMad-positive in controls. To this end, we examined co-expression of the reporter with anti-pMad and anti-Elav in controls and *wit* mutants. As predicted, we observed that reporter activity was primarily lost in neurons that are pMad-positive in controls (Supplementary Figure S1 and Table S4). We further validated that these reporters respond cell-autonomously to the canonical BMP pathway, by finding that reporter expression was reduced upon co-expression of *UAS-dad* and a dominant negative form of *tkv* (*UAS-tkv^{DN}*) in neurons, using the *elav-GeneSwitch-GAL4* driver (Supplementary Figures S7 and S8).

For the 13 reporters that failed to express in the VNC, we postulated that these genomic fragments may be missing critical regulatory elements required to drive neuronal reporter activity. To test this, we searched the Janelia GAL4 collection (60) for reporters of larger DNA fragment size that contain any of the genomic fragments tested. We found three ∼3 kb genomic fragments (*GMR49D01 GMR89G06* and *GMR89H02*) that encompass the *BMP-AE*s of *Van16*, *Van37* and *Van38*, respectively. Upon testing, all of these genomic fragments drove reporter expression in subsets of pMad-positive neurons, and two of these, *GMR89G06* and *GMR89H02*, exhibited reduced reporter expression in *wit* mutants (Supplementary Figure S6). We also considered the possibility that BMP signaling may directly repress the activity of these reporters. Therefore, we tested for de-repression of these remaining 10 reporters in *wit* mutants, but found that none of them increased expression in the absence of BMP signaling, suggesting that the *BMP-AE*s within these genomic fragments do not act as BMP-dependent *silencer elements* (Supplementary Figure S9).

Overall, we identified 34 genomic fragments responsive to the loss of neuronal BMP signaling in *wit* mutants, out of the 58 genomic fragments tested; giving our approach a discovery rate of 59%. These data provide experimental validation for a computational approach to efficiently identify genomic regions that contain *wit*-responsive neuronal enhancers, and further suggests that *BMP-AE*s serve as a common platform for BMP-responsive gene regulatory activity in VNC efferent neurons.

*BMP-AE*s recruit pMad/Medea complexes *in vitro* and are necessary for reporter expression *in vivo*

We tested if *BMP-AE*s embedded in *wit*-responsive fragments interact with pMad/Medea complexes. To this end, we analyzed the recruitment of an activated pMad/Medea complex to three *BMP-AE*s, by Electrophoretic Mobility Shift Assay (EMSA). These *BMP-AE*s were selected because they represent different sequences within the Medea *GNCV* consensus sequence, and because their corresponding genomic fragments reported broad activity that was strongly *wit*-responsive. *Drosophila* Schneider 2 cells (S2) were transfected with plasmids encoding *Mad* and *Medea* as well as constitutively activated *tkv*, *tkv^{QD}*. Lysates from these cells were tested for their ability to band shift IRDye700 tagged probes containing these *BMP-AE* sequences *in vitro* (Figure 3A, B). In all three cases, the *BMP-AE* probes recruited a pMad/Medea complex, as shown by

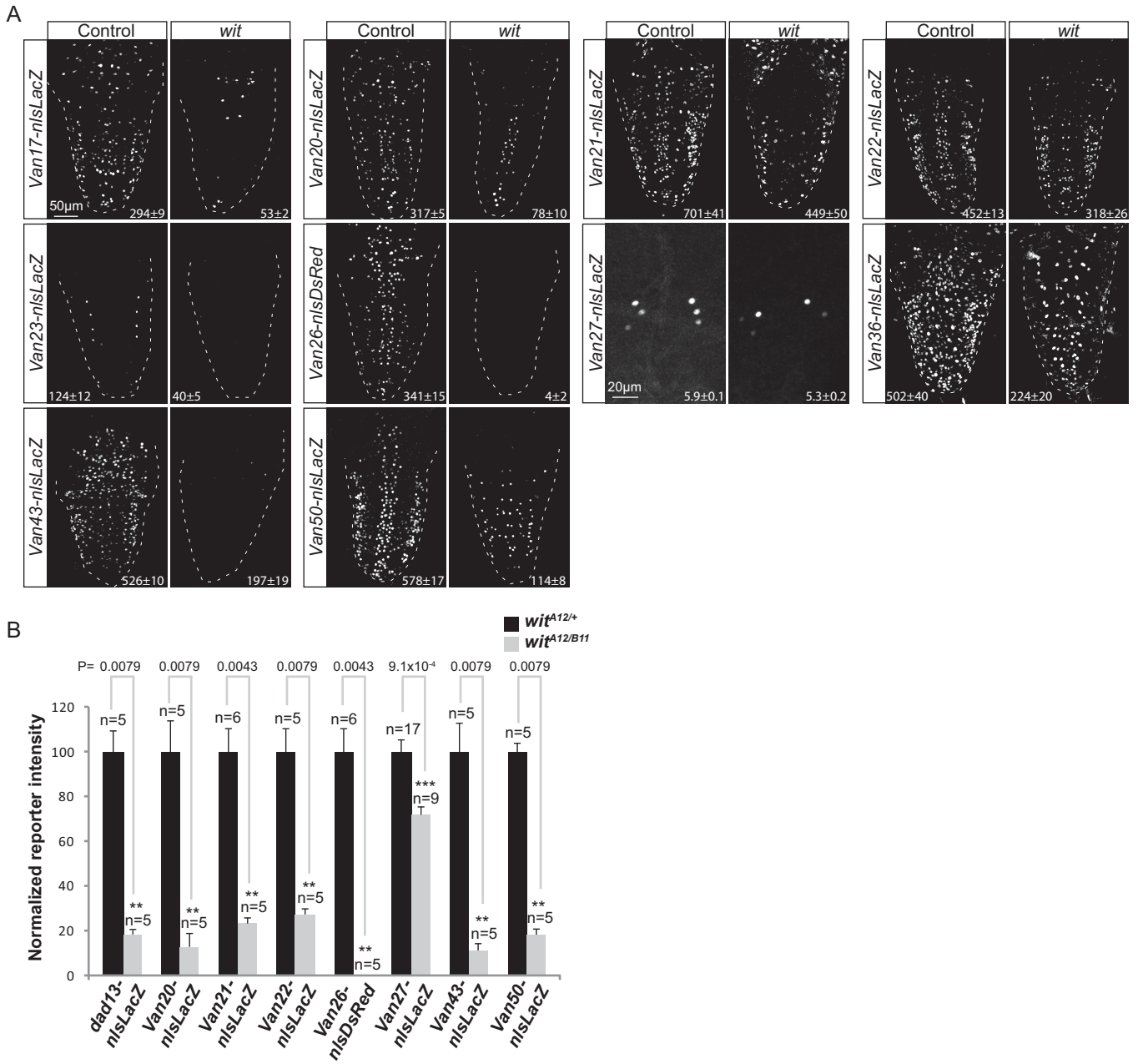

Figure 2. Identification of *wit*-responsive genomic fragments in neurons. (**A**) Nuclear β-galactosidase and nlsDsRed expression patterns driven from 10 genomic fragments containing conserved *BMP-AE*s that are down-regulated in *wit* mutants (wit^{A12}/wit^{B11}) as compared to controls ($wit^{A12}/+$), in dissected late third instar larval VNCs. The observed down-regulation ranged from a total loss of all expression to loss of expression in a subset of neurons. The mean ± SEM number of nuclei per VNC that express the reporter is indicated at the bottom of each panel. Reporter activity of all fragments was significantly reduced in *wit* mutants; *Van17*, $P = 5.83 \times 10^{-4}$; *Van20*, $P = 0.0079$; *Van21*, $P = 0.0087$; *Van22*, $P = 0.0159$; *Van23*, $P = 0.0022$; *Van26*, $P = 0.0022$; *Van27*, $P = 0.0154$; *Van36*, $P = 0.0022$; *Van43*, $P = 0.0012$; *Van50*, $P = 0.0079$ (two-sided Wilcoxon rank-sum test). At least five VNCs were analyzed for each genotype. (**B**) Quantification of relative nuclear β-galactosidase and nlsDsRed intensities for 8 of the 11 *wit*-responsive genomic fragments shown in Figures 1H–K and 2A that show expression in motor neurons of the dorsal midline and 6 ventral neuropeptidergic cells. Bar plots illustrate mean ± SEM; n indicates the number of VNCs analyzed. ***$P < 0.001$; **$P < 0.01$, *$P < 0.05$ (two-sided Wilcoxon rank-sum test).

a strong band shift of labelled probe. The sequence specificity of this recruitment was shown by competition assays, in which an excess of untagged wildtype probe fully competed for the labelled band shift, while an untagged probe with substitution mutations through the pMad binding site abolished competition, and a strong band shift was retained (Figure 3B).

The 62 *BMP-AE*s tested above display a high degree of diversity within the consensus *BMP-AE* motif. Differences within this consensus motif may contribute to differential affinity for pMad/Medea recruitment, and potentially underlie differences observed between *wit*-responsive and *wit*-non responsive genomic fragments. To test this, we selected 7 *BMP-AE*s from each set, based on their divergent Medea-

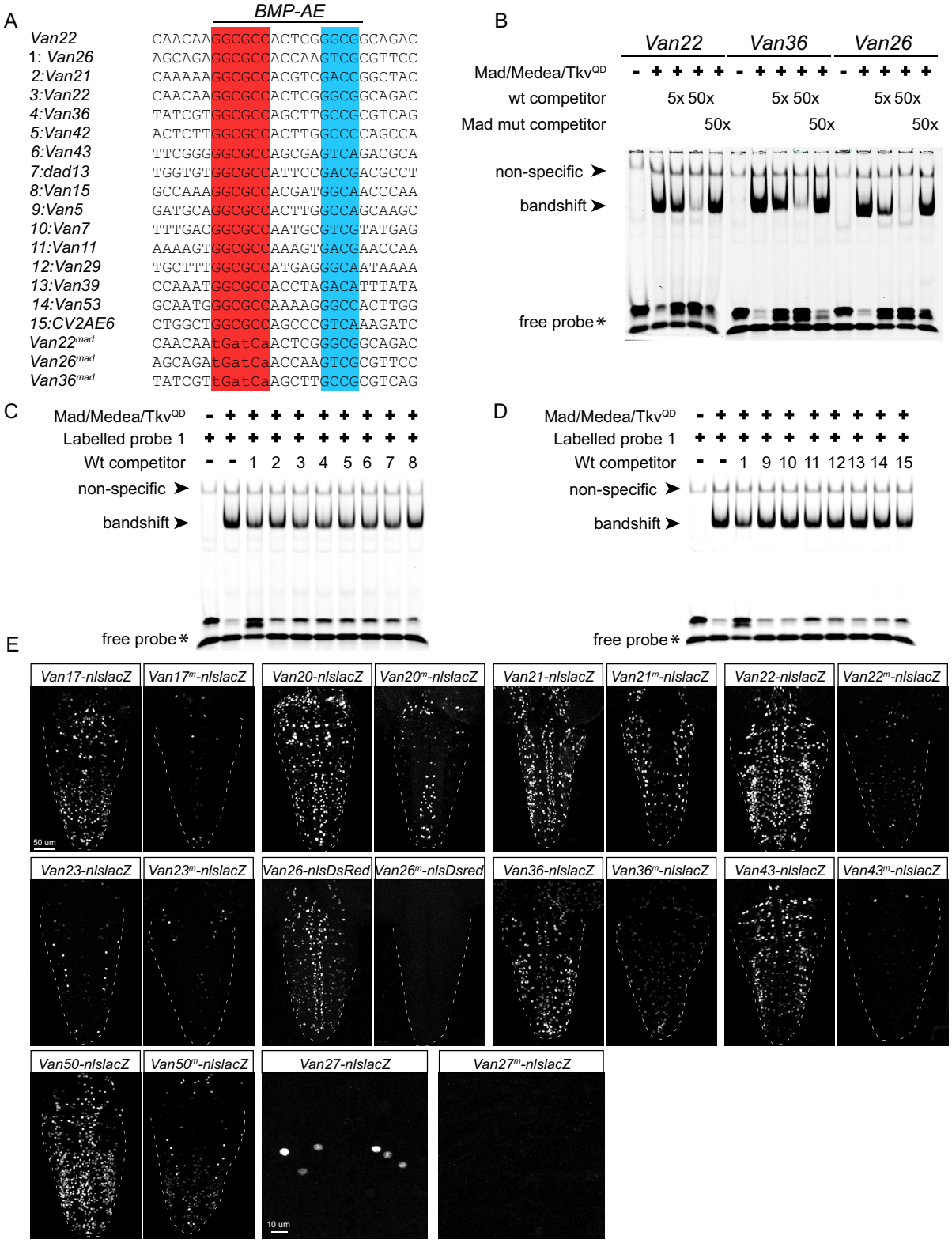

Figure 3. The *BMP-AE* of *wit*-responsive genomic fragments is bound by pMad/Medea complexes with high affinity *in vitro* and is required *in vivo*. (**A–D**) Electrophoretic mobility shift assays (EMSA) for three selected *BMP-AE*s with S2 cell lysates transfected with Mad, Medea and Tkv^{QD} to activate BMP signaling. (**A**) DNA sequences used for EMSA analysis, highlighting the presumptive pMad (red) and Medea (blue) binding sites of the *BMP-AE*. The DNA sequences shown were taken from the predicted *BMP-AE* within the indicated genomic fragments. The *BMP-AE*s within *Van22, Van36* and *Van26* were used as IRDye700-labeled probes, as well as for unlabeled wildtype and mutated ($Van36^{mad}$, $Van26^{mad}$, $Van22^{mad}$) competitors. All other sequences were used as unlabeled wildtype competitors. Mutant competitors were all mutated at the putative pMad-binding site. (**B**) EMSA with lysates from S2 cells transfected with the indicated plasmids (Mad/Medea/Tkv^{QD}) were incubated with the indicated IRDye700-labeled wildtype probes and run on non-

binding *GNCV* consensus sequence, and used these as untagged probes (in a 5:1 stoichiometry) to compete for the band shift generated from interaction of pMad/Medea with the *BMP-AE* from the *wit*-responsive *Van26* fragment (as above) (Figure 3C, D). Notably, five out of the seven *BMP-AE*s from *wit*-responsive fragments strongly competed for the labelled band shift, while two weakly competed. In contrast, five out of the seven *BMP-AE*s from *wit*-non responsive fragments failed to compete for the labelled band shift, while two weakly competed. Thus, *BMP-AE*s within *wit*-responsive fragments typically have a higher affinity for pMad/Medea complexes than those from *wit*-non responsive genomic fragments, indicating that pMad/Medea affinity may underlie observed differences in enhancer activity for the majority of *BMP-AE* containing genomic fragments.

These results prompted us to compare the sequences of all 59 *BMP-AE* motifs (excluding the three *BMP-AE*s of *Van10* and *Van19*, as above), embedded within the 56 genomic fragments for which we could determine responsiveness to *wit*. Interestingly, in comparing *BMP-AE*s from *wit*-responsive and *wit*-non responsive fragments, we found that *BMP-AE*s from *wit*-responsive fragments were significantly enriched for thymine at position 11 and depleted for guanine and adenine at position 11 and position 15, respectively (Supplementary Figure S10A, C). Although we could not detect any other sequence bias that could explain a difference of affinity between both sets of motifs, we noticed that a *GCCA* sequence within the Medea binding sequence is absent for *BMP-AE*s in *wit*-responsive fragments (0%, 0/37), whereas it is well represented for *BMP-AE* in *wit* non-responsive fragments (23%, 5/22) (Supplementary Figure S10C). These data led us to examine whether *BMP-AE* motifs that are active in the CNS differ from those that are active in other tissues. To do this, we compared the sequence of *BMP-AEs* within neuronal *wit*-responsive fragments to those that are embedded in genomic fragments shown to be *tkv*-responsive in the late embryo and wing imaginal disc (34) (Supplementary Figure S10B, C). Interestingly, we noticed that neuronally-active *BMP-AE*s were enriched for cytosine and depleted for guanine at position 8 in the linker region. Overall, these results demonstrate that that there are sequence biases that correlate with, and perhaps even confer pMad/Medea recruitment or even tissue-specific function, in positions previously found to not be critical in the *BMP-AE* motif. It will be interesting to analyze a larger set of *BMP-AE* motifs to demonstrate whether these biases are indeed functionally relevant.

We next tested whether the activity of the identified *wit*-responsive fragments was dependent on the embedded *BMP-AE*s. For ten selected *wit*-responsive fragments, we introduced specific mutations into the pMad site of the *BMP-AE*, and placed mutant genomic fragment reporters into the same insertion site as the corresponding wildtype reporter. In all cases tested, reporter expression driven from the mutant genomic fragments was lost in pMad-positive neurons, in a pattern that was strikingly similar to that observed for wildtype *wit*-responsive fragments in *wit* mutants (Figure 3E). These data strongly suggest that the *BMP-AE* motif serves as the platform for pMad/Medea-responsive reporter activity of these genomic fragments. We hereafter refer to these as functional *BMP-AE*s.

Identification of neuronal genes directly regulated by the BMP signaling pathway

The large collection of *wit*-responsive fragments identified suggested that a battery of genes may be directly regulated by BMP-activated pMad/Medea transcriptional regulation in efferent neurons. We next sought to resolve if the identified *wit*-responsive fragments are near BMP-responsive genes. Therefore, we dissected VNCs from control and *wit* mutant third instar larvae and compared transcript expression by RNA-sequencing (RNA-seq) of total poly-A transcripts. To evaluate the sensitivity of the technique and validate our approach, we examined the relative transcript level of five BMP-responsive neuronal genes with highly restricted expression; *FMRFamide* (*FMRFa*), *Partner of bursicon* (*Pburs*), *Crustacean cardioactive peptide* (*CCAP*), *Myoinhibiting peptide precursor* (*Mip*) and *Insulin-like peptide 7* (*Ilp7*) (10,11,13). In the VNC, these genes all exhibit *wit*-dependent expression in a small subset of the neurons in which the gene is expressed. In spite of this, our RNA-seq analysis successfully identified all genes as being significantly downregulated in *wit* mutants, indicating that our RNA-seq analysis is sufficiently sensitive to identify neuronal subtype-specific *wit*-responsive gene regulation (Supplementary Table S2).

We next examined whether *BMP-AE*s in *wit*-responsive fragments were preferentially enriched over *BMP-AE*s within *wit*-non responsive fragments around *wit*-responsive genes. To avoid over-counting genomic regions where

denaturing gels. A band shift of each labeled probe was generated only in lanes loaded with S2 cell lysate transfected with Mad/Medea/Tkv^{QD}. Labeled probes were mixed with 5x or 50x stoichiometric excess of wildtype competitor (wt) or mutated (Mad mut) competitor. Five and 50x excess of wildtype competitor progressively diminished the band shift of the labeled probe, indicative of pMad/Medea complexes binding to the unlabeled competitor. In contrast, addition of the mutated competitor at a 50x excess resulted in retention of the labeled band shift, indicating that mutated competitors did not bind pMad/Medea complexes. (**C, D**) We tested the ability of fourteen *BMP-AE*s from *wit*-responsive (1–8 in **A**) and *wit*-non responsive (9–15 in **A**) genomic fragments to compete for pMad/Medea binding, as unlabeled DNA probes, with an IRDye700-labeled DNA probe for the *BMP-AE* of *Van26*. EMSA with lysates from S2 cells transfected with the indicated plasmids (Mad/Medea/Tkv^{QD}) were incubated with the IRDye700-labeled *Van26* probe and the fourteen *BMP-AE* DNA unlabeled competitors. The labeled probe was mixed with a 5× stoichiometric excess of unlabeled competitors. The 5× excess of *Van26* competitor diminished the band shift of the labeled probe, indicative of pMad/Medea complexes binding to the unlabeled competitor. The 5× excess of functional *BMP-AE*s within *Van21*, *Van22*, *Van36*, *Van42*, *Van43*, *dad13* and *Van15* competitors also resulted in a diminution of the band shift of the labeled probe (**C**). In contrast, the 5x excess of non-functional *BMP-AE*s within *Van5*, *Van7*, *Van29*, *Van39* and *Van53* did not result in a diminution of the band shift of the labeled probe (**D**), indicating that their affinity for the pMad/Medea complexes is lower than for the functional *BMP-AEs* within *wit*-responsive fragments. (**E**) Nuclear β-galactosidase and nlsDsred expression driven from 10 select *wit*-responsive fragments in which the *BMP-AE* motif was either wildtype or mutated at the Mad site. The point mutations that were introduced into the Mad site of the *BMP-AE*s are similar to the ones that abolished competition *in vitro*. In all cases, there was a reduction in the number of nuclei that expressed the *nlsLacZ* and *nlsDsred* reporters.

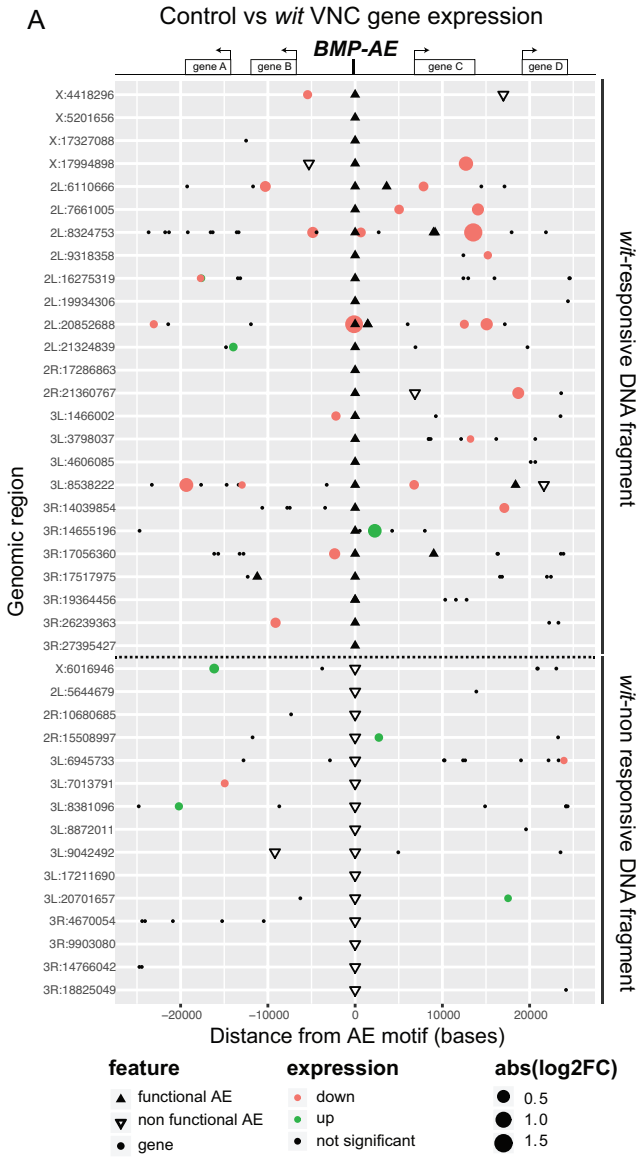

B

	10 kb	20 kb	30 kb	40 kb	50 kb
AE *wit*- responsive	36% (9)	60% (15)	60% (15)	64% (16)	68% (17)
AE non *wit*-responsive	0% (0)	7% (1)	13% (2)	33% (5)	47% (7)
Bcd-responsive	11% (3)	27% (7)	31% (8)	35% (9)	46% (12)

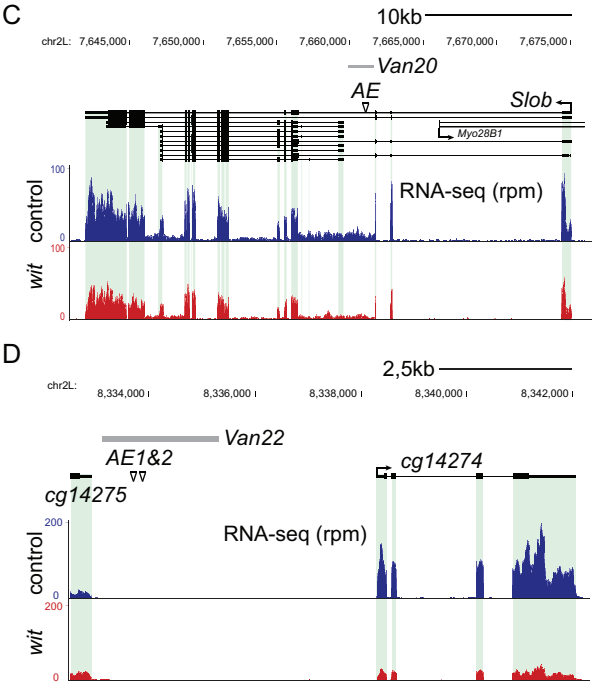

Figure 4. Proximity of *BMP-AE*s to BMP-regulated genes. (**A**) Diagram showing genomic regions (version Dm6) containing *BMP-AE*s analyzed for *wit*-responsiveness (see Supplementary Table S1 and Table S2 for identity of all *BMP-AE*s, genomic fragments and *wit*-responsive genes). We do not show 5 of the *BMP-AE*s tested, for the sake of clarity. Black triangles denote *BMP-AE*s within *wit*-responsive fragments; a subset of these represent two closely spaced *BMP-AE*s (on lines 2L:8324753, 2L:20852688 and 3R:19364456). Open inverted triangles denote *BMP-AE*s within *wit*-non responsive genomic fragments. Circles denote the 5′-most transcription start site (TSS) of genes expressed in the VNC, within a span of 25 kb from the central *BMP-AE* shown; small black circles are genes that are *wit*-non responsive, red and green circles are genes that are significantly reduced or upregulated, respectively, in *wit* mutants; as determined by RNA-seq analysis of control (wit^{A12}/+) and *wit* mutant (wit^{A12}/wit^{B11}) VNCs. The size of red/green circles denotes absolute log2-fold change from control to *wit* mutants expression level. (**B**) Proximity to the TSS of BMP-activated genes of *BMP-AE*s within *wit*-responsive (*AE* wit-responsive) and non-responsive genomic fragments (*AE non wit*-responsive), and also Bicoid-responsive fragments (*Bcd*-responsive). The percentage (to total number of genomic regions) and the actual number of genomic regions containing each motif type that are within a specific distance to the TSS of at least one BMP-activated gene is shown. The enrichment for functional *BMP-AE*s over non-functional *BMP-AE*s or Bcd-responsive fragments are shown at 10–50 kb increments. (**C, D**) The genomic locus of two genes, *Slob* (**C**) and *CG14274* (**D**) that were reduced in *wit* mutants, as well as the span of the genomic fragments tested (*Van20* in **C**, and *Van22* in **D**), and also the specific location of the *BMP-AE*s therein is shown. RNA-seq rpm denotes the number of reads per million reads.

multiple *BMP-AE* motifs clustered around multiple *wit*-responsive genes, we instead quantified the number of genomic regions in which any number of *BMP-AE*s were up to 50 kb from the TSS (transcription start site) of any number of *wit*-responsive genes (Figure 4A, B, Supplementary Table S2). As an additional control, we examined enrichment of Bicoid (Bcd)-responsive genomic fragments to *wit*-responsive genes (Supplementary Figure S11A). These fragments are active during anterior-posterior patterning of the early *Drosophila* embryo (76) and are not predicted to enrich around *wit*-responsive neuronal genes. Our analysis was performed separately for BMP-activated genes (significantly downregulated in *wit*) versus BMP-repressed genes

(significantly upregulated in *wit*) (see Materials and Methods for details of analysis).

Out of the 25 genomic loci that contain all of the 34 *wit*-responsive fragments (Figure 4A), we found that 36% of these loci (9/25) contain *BMP-AE*s within 10 kb of a BMP-activated gene's TSS, which increases to 60% (15/25) at 20 kb and then plateaus to reach 68% (17/25) at 50 kb (Figure 4B). For enrichment analysis of *BMP-AE*s within the 22 *wit*-non responsive fragments, we wished to eliminate the possible confound that the presence of a nearby *wit*-responsive fragments may explain the *wit*-responsiveness of the gene. Therefore, we only considered those regions that did not also include a *wit*-responsive fragment, which eliminated *BMP-AE*s within 4 *wit*-non responsive fragments. Thus, we examined 15 genomic loci containing the remaining 18 *wit*-non responsive fragments, and found that 0% of these loci (0/15) contain *BMP-AE*s within 10 kb of a BMP-activated gene's TSS, with only 7% (1/15) at 20 kb and steadily increasing to 47% (7/15) at 50 kb (Figure 4B). Similarly, only 11% of the loci (3/26) that contain Bcd-responsive fragments were within 10 kb of a BMP-activated gene's TSS, with 27% (7/26) by 20 kb and rising to 46% (12/26) by 50 kb (Figure 4B and Supplementary Figure S11A). These data indicate that functional *BMP-AE*s are selectively enriched within 20 kb of at least one BMP-activated gene (circled in red in Figure 4B). Indeed, at 20 kb this difference was found to be significant by chi2 analysis; $P = 2.7 \times 10^{-3}$ comparing *wit*-responsive versus *wit*-non responsive fragments, and $P = 3.6 \times 10^{-2}$ comparing *wit*-responsive versus Bcd-responsive fragments. We next tested for any enrichment of BMP-repressed genes at the same distance, and found no significant difference between *BMP-AE*s within *wit*-responsive fragments (12%: 3/25) and *wit* non-responsive fragments (20%: 3/15; $P = 0.82$), nor Bcd-responsive fragments (19%: 5/26; $P = 0.75$) (Supplementary Figure S11B). These results indicate that functional *BMP-AE*s are selectively enriched near BMP-activated genes, supporting the hypothesis of a positive regulatory relationship.

Since *Drosophila* embryonic enhancers most often regulate the adjacent gene (59), we addressed whether functional *BMP-AE*s enrich to adjacent *wit*-responsive genes, i.e. with no intervening *wit*-non responsive gene. We calculated the proportion of genomic loci containing a *BMP-AE* whose adjacent gene was a BMP-activated gene. For this analysis, we were able to examine 26 loci for *BMP-AE*s in *wit*-responsive fragments (as opposed to the 25 shown above) (see Methods and Materials for details). Notably, 61% (16/26) of genomic loci containing functional *BMP-AE*s harbor at least one adjacent BMP-activated gene. In contrast, only 7% (1/15) and 11% (3/26) of genomic loci containing non-functional *BMP-AE* ($P = 1.9 \times 10^{-3}$ compared to *wit*-responsive fragments) and Bcd-responsive fragments ($P = 5.5 \times 10^{-4}$ compared to *wit*-responsive fragments), respectively harbor at least one adjacent BMP-activated gene. These data suggest that a large proportion of functional *BMP-AE*s regulate the adjacent gene.

We observed numerous instances of multiple, reiterated *BMP-AE*s within 12 kb of a single annotated gene locus; therefore, we compared the proximity of individual versus reiterated *BMP-AE*s to BMP-activated genes. We found that 77% of reiterated *BMP-AE*s (10/13) were within or adjacent to BMP-activated genes, and that 46% (6/13) of single *BMP-AE*s were within or adjacent to BMP-activated genes. This corroborates our finding that 72% of reporters (21/29) from a locus with reiterated *BMP-AE* were *wit*-responsive, whereas 48% of reporters (13/27) containing a single *BMP-AE* were *wit*-responsive. These data indicate that reiteration of conserved *BMP-AE*s in a locus is a strong predictor of a *wit*-responsive genomic region and nearby *wit*-responsive genes in the *Drosophila* nervous system, but that the presence of multiple *BMP-AE*s within a gene locus is not a requirement for the *wit*-responsiveness of a genomic region.

Many genes have numerous alternate promoters that generate different transcript isoforms; therefore, we considered the possibility that *BMP-AE*s may selectively regulate specific isoforms of a gene, and not others. To test this hypothesis, we analyzed our RNA-seq dataset for differentially expressed transcripts within 100 kb of functional *BMP-AE*s. Interestingly, we found six instances that confirmed our hypothesis (Supplementary Table S2). For example, the *sickie* gene (*sick*) locus contains eight predicted promoters that generate twelve putative isoforms. We found that only the two shortest isoforms were significantly down-regulated in *wit* mutants, whereas the expression of other isoforms remained unchanged (Supplementary Figure S12). Interestingly, a functional *BMP-AE* (*Van25*) was located approximately 950bp upstream of the TSS of each differentially expressed isoform, suggesting specific isoform regulation by this *BMP-AE*.

In summary, these data suggest that *BMP-AE*s identified here are pMad/Medea-responsive *cis*-elements for the BMP-activation of a battery of genes and selective gene isoforms. Moreover, a subset of these genes are known to be regulators of synaptic growth and neurotransmission, suggesting that they are putative effectors of the BMP signaling pathway in neurons (see **Discussion**).

*BMP-AE*s are required for BMP-activated *twit* expression *in vivo*

To obtain additional evidence that identified *BMP-AE*s represent genuine *cis*-regulatory sites for BMP-responsive gene expression, we focused on the BMP-activated gene, *twit*, which plays an effector role in BMP-dependent neurotransmission at the larval NMJ (23,25). The *twit* locus harbors three conserved *BMP-AE*s; one in the 5′UTR (*AE1* within the *Van26* fragment) and two *BMP-AE*s (sharing a single *GGCGCC* palindromic Mad motif) are located in the first intron of *twit* (*AE2&3* within the *Van27* fragment) (Figure 5A). Our reporter analysis in Figures 2 and 3 suggested that the *AE1* is required for widespread *wit*-responsive *twit* expression in motor neurons, whereas the inverted *AE2&3* motifs are only required for *wit*-responsive *twit* expression in six ventral neurons (Supplementary Table S4). To examine whether either *BMP-AE*s mediate the *wit*-responsiveness of *twit*, we first compared reporter expression driven from *Van26* and *Van27* with that of *twit-GFP*, a Mi{MIC} transposon gene trap insertion in the *twit* intron (57). Notably, we observed that *Van26* mostly recapitulated the extensive expression of *twit-GFP* expression in motor

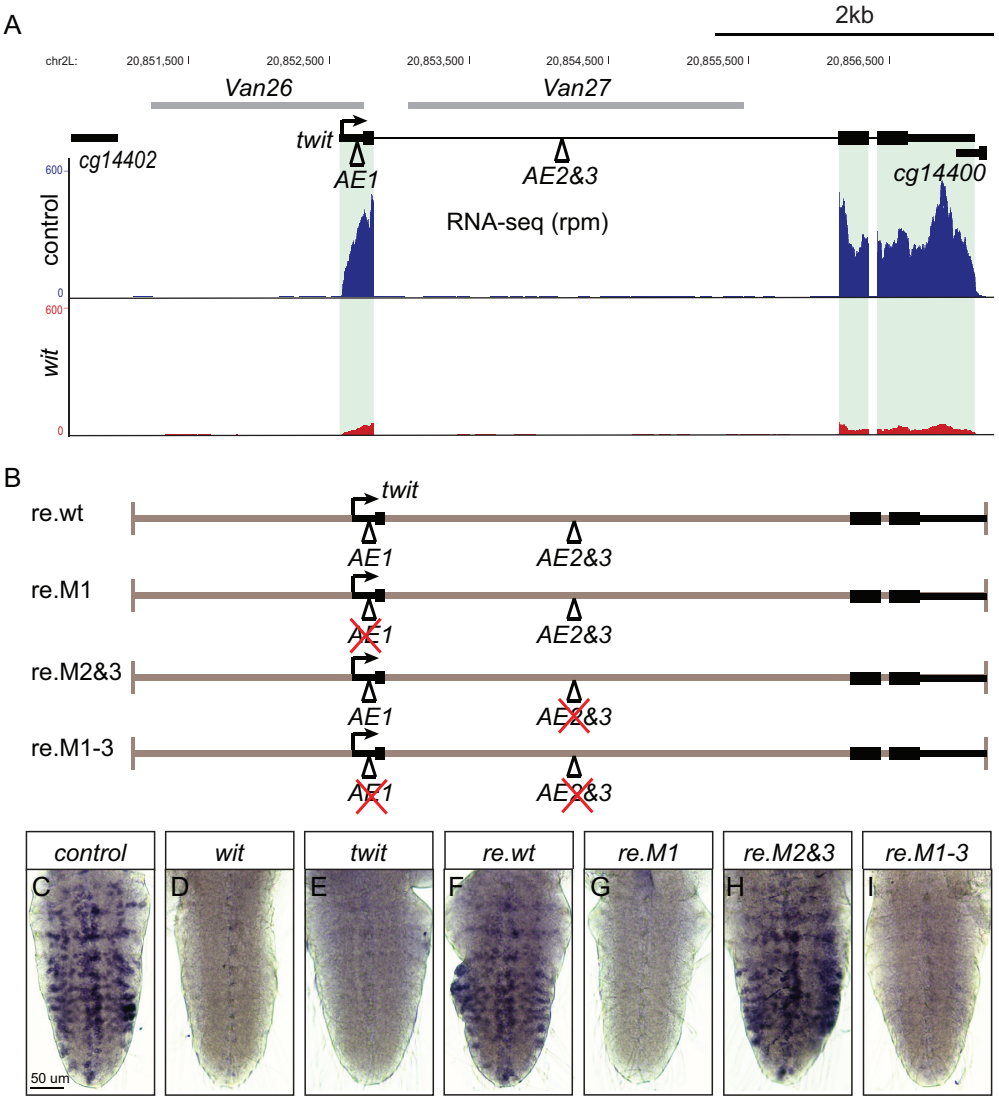

Figure 5. An exonic *BMP-AE* is required for *twit* transcription in motor neurons. (**A**) Genome browser showing the *twit* locus with three *BMP-AE*s and the two genomic fragments used for the reporter analysis, together with the tracks from RNA-seq (in rpm; reads per million reads). The expression of *twit* is strongly downregulated in wit^{A12}/wit^{B11} mutants as compared to controls ($wit^{A12}/+$). (**B**) Schematic of four *twit* locus DNA constructs used for *in vivo* rescue of *twit* mutants shown in **F–I**. The *BMP-AE*s within this locus as well the *BMP-AE* motifs mutated in each construct are shown. (**C–I**) *In situ* hybridization using a Digoxigenin-labeled RNA *twit* probe reveals expression of *twit* in VNCs of controls (**C**), *wit* mutants (**D**), *twit* mutants (**E**) and *twit* mutants rescued with the constructs shown in B (F-I). The *AE*1 within the *twit* 5′UTR is critical for *twit* motor neuron expression. Genotypes: (**C**) w^{1118}. (**D**) w^{1118};; wit^{A12}/wit^{B11}. (**E**) w^{1118}; $twit^{160}$ / $twit^{160}$. (F) w^{1118}; $twit^{160}$ / $twit^{160}$; *re.wt*/+. (**G**) w^{1118}; $twit^{160}$ / $twit^{160}$; *re.M1*/+. (**H**) w^{1118}; $twit^{160}$ / $twit^{160}$; *re.M2&3*/+. (**I**) w^{1118}; $twit^{160}$ / $twit^{160}$; *re.M1-3*/+.

neurons, while *Van27* recapitulated the expression of *twit-GFP* expression in six ventral neuropeptidergic cells in the VNC (Supplementary Figures S5, S13A, B). Interestingly, expression driven by *Van26* and *Van27* did not overlap (Supplementary Figure S13C). This suggests that the *AE1* within *Van26* is required for widespread *wit*-responsive expression of *twit* in motor neurons, whereas *AE2&3* within *Van27* are only required for *twit* expression in six ventral neuropeptidergic cells of the VNC.

To test whether these *BMP-AE*s are required for *twit* expression, we generated a series of rescue transgenes containing ∼6 kb of genomic DNA encompassing the *twit* locus, and targeted these into the *attP2* integrase site in *twit* deletion mutant flies. Rescue transgenes included the wildtype sequence (*re.wt*) and also a series of *BMP-AE* mutants, to eliminate pMad/Medea recruitment, including single mutants of *AE1* (*re.M1*) and *AE2&3* (*re.M2&3*), and also a double mutant of *AE1* and *AE2&3* (*re.M1-3*) (Figure 5B). Flies transgenic for these constructs were analyzed for neuronal *twit* transcript expression by *in situ* hybridization. We confirmed that *re.wt* rescued *twit* expression of *twit* mutants throughout the VNC (Figure 5C–F). In contrast, both *re.M1* and *re.M1-3* failed to rescue detectable VNC *twit* expression in *twit* mutants (Figure 5G, I), whereas *re.M2&3* rescued broad *twit* transcript levels in *twit* mutants (Figure 5H). Thus, the single *BMP-AE* in the *twit* 5′ UTR is required for native *wit*-responsive motor neuron expression of *twit in vivo*. We could not detect any *twit* expression in

the six ventral neuropeptidergic cells using *re.M1*, suggesting that the *BMP-AE1* found in the *twit* 5′UTR also contributes to *twit* expression in these cells, or reflects the insufficient resolution of the *in situ* hybridization protocol to efficiently detect expression in these six cells. Regardless, we identified the *BMP-AE* motif that acts as the primary functional pMad/Medea-responsive element for *wit*-responsive *twit* expression in motor neurons.

The neuronal function of the *BMP-AE* is evolutionarily conserved

Our analysis identifies a number of *cis*-regulatory motifs and genes that represent part of the BMP network in neurons of the fly VNC. This prompted us to test the hypothesis that together with pMad and Medea, the *BMP-AE* forms a fundamental regulatory circuit in the nervous system of distantly related animals. To test this, we used two approaches. First, we generated a reporter containing 8× concatenated *BMP-AE* sequences taken from the *Drosophila dad* gene locus (*dad13*) (Figure 6A), placed upstream of a minimal thymidine kinase (Tk) gene promotor and enhanced GFP (EGFP) reporter gene (termed *BMP-AE8x-EGFP*). This reporter was electroporated into the developing chick spinal cord at stage HH14 and its activity was analyzed after 24 and 48 h. At 24 h, one day post-electroporation (dpe), the *EGFP* reporter was robustly expressed in the dorsal-most region of the spinal cord, where BMP signaling is highest during a period of active patterning of the dorsal neuronal subtypes (Figure 6B) (85,86). At 2 dpe, reporter expression was also detected in medial to ventral regions of the developing neural spinal cord, which is consistent with previous observations (85) (Supplementary Figure S14). To test whether the observed dorsal *BMP-AE8x-EGFP* reporter activity was BMP-dependent, we first tested the activity of a *BMP-AE8x-EGFP* reporter mutated at each pMad-binding site (*BMP-AE8x*$^{\Delta mad}$*-EGFP*) (Figure 6A). This eliminated reporter activity at both 1 dpe and 2 dpe (Figure 6B and Supplementary Figure S14). Second, we co-electroporated the *BMP-AE8x-EGFP* and *BMP-AE8x*$^{\Delta mad}$*-EGFP* reporters with a phospho-mimetic (constitutively activated) form of Smad1 (Smad1 S/D) (85), which is a vertebrate ortholog of *Drosophila* Mad. We found that the *BMP-AE8x-EGFP* reporter expression greatly increased and expanded throughout the neural tube, but the *BMP-8xAE*$^{\Delta mad}$*-EGFP* reporter expression was unresponsive and exhibited no activity (Figure 6C, D). We conclude that the *Drosophila BMP-AE* sequence is directly activated by BMP/pSmad1 signaling in the developing chick neural tube.

To further test the hypothesis that functional DNA motifs similar to the *BMP-AE* are conserved in vertebrates, we replaced the sequence of the *BMP-AE1* within the *Van26* reporter with a 15 bp motif taken from a BMP-responsive enhancer (BRE) of the *Xenopus laevis bambi* gene (termed *Van26*$^{bambi\text{-}BMP\text{-}AE}$*-nlsDsRed*) (Figure 6E) (87). Even though no such exact *BMP-AE* sequence was tested in our reporter analysis, this motif perfectly matches the *Drosophila BMP-AE* consensus. Notably, this *bambi BMP-AE* motif functionally replaced the wildtype *BMP-AE1*, as strong reporter activity was observed in 383 ± 10 nuclei per VNC (n = 5) The pattern of expression was strikingly similar to that of *Van26*, which was expressed in 341 ± 15 nuclei per VNC (n = 6) (Figure 6F). Moreover, reporter activity of the *Van26*$^{bambi\text{-}BMP\text{-}AE}$*-nlsDsRed* reporter was reduced to 10 ± 2 nuclei per VNC (n = 5; P = 0.0079) in *wit* mutants, which is comparable to the reduction of reporter expression observed for the wildtype *Van26* reporter, which was in 4±2 nuclei per VNC (n = 6; P = 0.0022) (Figures 2, 6F).

Taken together, these data show that the fundamental transcriptional mechanisms acting downstream of neuronal BMP signaling are conserved from *Drosophila* to vertebrates. It further suggests that the *BMP-AE* motif may be useful in future studies to predict and identify direct BMP-responsive genes and enhancers in vertebrate neurons.

DISCUSSION

BMP signaling acts via the transcriptional activity of pMad to control neuronal differentiation and synaptic function in *Drosophila* (9–11,13–15,22,26). BMP signaling plays similarly critical roles throughout vertebrate nervous system development, function and repair (88–94). Yet, how BMP-responsive transcription coordinates diverse gene regulatory programs in the nervous system remains poorly defined in any system. To start defining these transcriptional programs in the nervous system, we have demonstrated the utility of a combined computational and transgenic approach in predicting and validating 34 novel direct *wit*-responsive genomic fragments in motor and neuropeptidergic neurons of the *Drosophila* VNC. Together with differential transcript profiling, we showed that the *BMP-AE* motifs within these *wit*-responsive genomic fragments are enriched around BMP-activated genes, indicative of putative regulatory pairings that we validated for the *twit* gene. Overall, our data provide insight into the organization of directly BMP-driven gene networks in neurons that control neuronal identity and synaptic function. In addition, we provide the largest verified collection of genomic fragments whose underlying enhancers are targeted by a developmental signaling pathway in neurons; offering a resource for detailed analysis of gene regulatory mechanisms underlying synaptic growth and function.

Prediction and validation of a large collection of direct BMP-activated neuronal enhancers

Since the discovery of a role for retrograde BMP signaling in motor and neuropeptidergic neurons, only two *wit/pMad*-responsive enhancers have been functionally verified *in vivo,* namely the *Tv4* enhancer of *FMRFa* and a proximal promotor region of *trio* (24,26). The Tv4 enhancer is only expressed in the six Tv4 neurons of the VNC (95,96). It contains a 39 bp *wit*-responsive *cis*-element with a *GGCGCC* pMad binding site that is required for enhancer function (26); however, there is no consensus *BMP-AE* within this *wit*-responsive *cis*-element. In addition, the promotor region of *trio* was immunoprecipitated by Myc::Mad in *Drosophila* embryonic motor neurons, and also shown to be responsive to BMP signaling in human embryonic kidney 293 cells; however, this region does not contain a

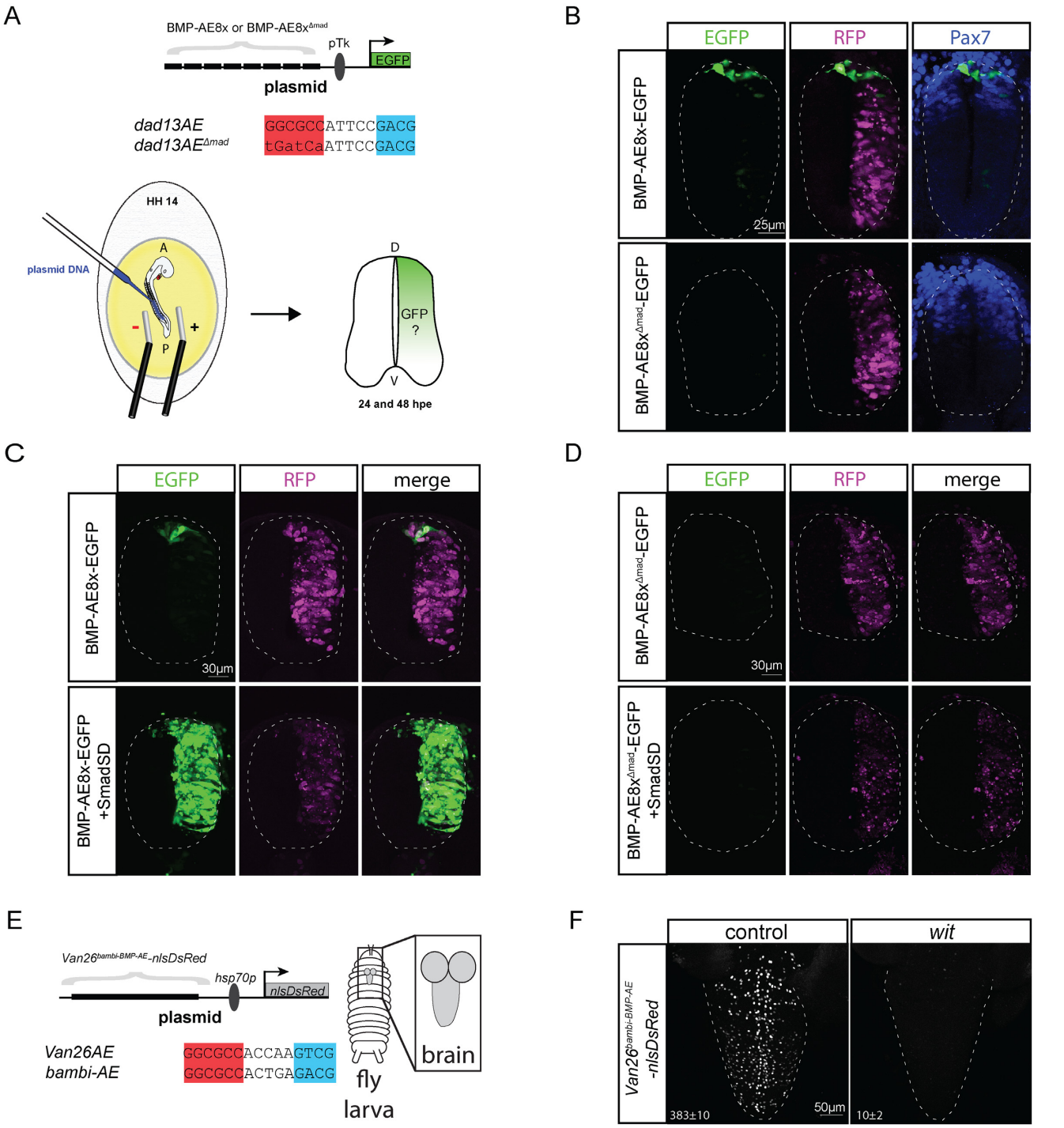

Figure 6. The *BMP-AE* mediates a conserved Smad-responsive function in the *Drosophila* and vertebrate CNS. (**A**) Schematic representation of the chick neural tube electroporation experiment with the sequence of the wildtype and mutated *dad13-BMP-AE*. (**B**) Expression of an octamerized version of a wildtype and mutated *BMP-AE* with an EGFP reporter at 24 hpe. The wildtype reporter displays strong EGFP expression in dorsal-most part of the neural tube, whereas the mutant reporter does not show any activity. An RFP control plasmid is co-electroporated with the EGFP reporters to indicate the efficiency of electroporation. Pax7 immunostaining indicates the dorsal region of the spinal cord. (**C, D**) Co-electroporation of a phosphomimetic form of Smad1 (Smad S/D) strongly increases and expands expression of the wildtype *BMP-AE* throughout the whole neural tube (**C**), but does not activate expression of the mutated version (**D**). (**E**) Schematic representation of the *Drosophila* transgenesis experiment where the *Van26* genomic fragment has its *BMP-AE* motif replaced with a *BMP-AE* taken from the *X. laevis bambi* enhancer. (**F**) Nuclear DsRed expression driven from the $Van26AE^{bambi\text{-}BMP\text{-}AE}$-*nlsDsRed* reporter in control and *wit* mutants third instar larval VNCs. The mean±SEM number of nuclei per VNC that express the reporter is indicated at the bottom of each panel. Reporter activity was significantly reduced in *wit* mutants ($P = 0.0079$ two-sided Wilcoxon rank-sum test). At least five VNCs were analyzed for both genotypes.

BMP-AE motif nor was a specific pMad/Medea-responsive *cis*-element pinpointed (24). Therefore, it has been uncertain whether canonical pMad/Medea-binding motifs have widespread activity in neurons or whether pMad/Medea-binding motifs are highly diversified in a way that might be expected to reflect the high diversity of neuronal subtypes and their subtype-specific gene expression profiles.

In this study, we chose the *BMP-AE* for our computational approach because its 15 bp sequence offered a high stringency parameter for genomic searches that had previously been used to successfully identify a number of BMP-responsive genomic fragments throughout development (34). We showed that the *BMP-AE* is a widely deployed activator of gene expression in neurons, often acting as the single necessary pMad/Medea-responsive *cis*-element within a genomic fragment. Thus, we have demonstrated that such *cis*-elements can be exploited for BMP-responsive enhancer discovery in *Drosophila* neurons. Also, the motif confidence method used here has previously proven a successful approach to the prediction of functional transcription factor and miRNA binding motifs (43,44). In this study, we used high stringency parameters testing *BMP-AE*s with a motif confidence high score of 0.8 or above. Because the function of the *BMP-AE* in the developing embryo is tolerant to modest changes in the linker length between the pMad and Medea binding motifs (34,39) and that many poorly conserved or degenerate *cis*-elements are fully functional (97–99), it will be interesting to test *BMP-AE*s with lower motif confidence score. This will allow us to assess conservation levels that still efficiently discover functional BMP-responsive motifs, albeit at the potential expense of a lower rate of success in identifying functional *BMP-AE*s.

In addition to the 34 *wit*-responsive fragments, we found that 24 of the genomic fragments tested exhibited no apparent *wit*-responsive expression in late third instar VNC neurons. This lack of *wit*-responsiveness may be the result of the low affinity of individual *BMP-AE* motifs for pMad/Medea complexes. Our *in vitro* analysis demonstrated that *BMP-AE*s within *wit*-responsive fragments typically have a higher affinity for an activated Mad/Medea complex than those within *wit*-non responsive fragments. These differences likely reside in sequence preferences for pMad/Medea recruitment, within the overall *BMP-AE* consensus. However, while we could not find any sequence signatures that explain the difference in affinity for all the *BMP-AE* motifs tested, we did observe a significant over-representation of specific nucleotides at positions 11 and 15 of functional and non-functional *BMP-AE*s, respectively. While these data suggest that there are underlying sequence preferences for pMad/Medea recruitment that confer apparent differences in *in vivo* enhancer activity, additional studies will be required to fully define these. We expect that better definition of the *BMP-AE* motif would lead to an increase in the efficiency of computational discovery of novel functional *BMP-AE*s.

Numerous *BMP-AE*s within the 24 *wit*-non responsive fragments display high affinity to the pMad/Medea complex. There are numerous lines of evidence or reasoning to suggest that a fraction of these *BMP-AEs* are indeed functional: (i) The BMP-activated *cv-2* gene is flanked by the *Van15/CV2-AE5 wit*-responsive fragment and the *CV2-AE6 wit*-non responsive fragment (Figure 4A; 2R:21360767). Interestingly, the *CV2-AE6* fragment has *tkv*-responsive enhancer activity in cells of the dorsal vessel and in an ectodermal stripe in embryos (30). Together with our data in the VNC, this suggests that *cv-2* is regulated by two distinct BMP-activated enhancers in the late embryo and third instar VNC. This may be a clear example where a single gene is regulated by an array of autonomous enhancers acting in a modular fashion to confer a variety of cell type- and temporal-specific expression patterns (46,100–102). Correspondingly, we found that several non-functional *BMP-AE*s are located in close proximity to functional *BMP-AE*s and a BMP-activated gene(s). Thus, several of these *wit*-non responsive *BMP-AEs* may provide pMad/Medea-regulated gene expression in different tissues. (ii) A lack of *wit*-responsiveness for a number of genomic fragments may also arise as a result of missing critical *cis*-regulatory elements required for *BMP-AE* to function. Indeed, *cis*-regulatory elements that act combinatorially to control gene expression can be spread over large distances that cannot be readily captured within the short 2kb fragments tested here (102). Accordingly, we found that two genomic fragments, *Van37* and *Van38*, only exhibited *wit*-responsive enhancer activity in the context of a larger fragment, fortuitously available through the Janelia GAL4 collection (60). (iii) It is also possible that additional *cis*-regulatory elements recognized by other transcription factors, or alternatively multiple linked enhancers within the same genomic fragment, compensate for the loss of BMP signaling in *wit* mutants to support the retention of genomic fragment activity.

The diversity of *BMP-AE* enhancer activities in the *Drosophila* nervous system

The 34 *wit*-responsive fragments discovered here display highly diverse expression patterns; some expressing broadly and others with restricted subtype-specific expression. Given our demonstration that the *BMP-AE* itself is necessary for the *wit*-responsive activity of these reporters, these results strongly suggest that pMad/Medea acting at this common *BMP-AE* motif must functionally collaborate with other subtype-specific transcription factors bound to flanking *cis*-elements, in order to generate these diverse expression patterns. We previously showed that the *FMRFa* gene is activated by a combinatorial code of pMad and a set of subtype-specific transcription factors (10,26,103,104), and reported that this integration occurs through the combined activities of distinct pMad and Apterous-binding *cis*-elements in the Tv4 enhancer of the *FMRFa* gene (26). This would be consistent with many other studies showing that the cell-specific activities of BMP-activated Smad complexes are often shaped by their functional interactions with local subtype-specific transcription factors in multiple organisms (105,106). It will be of great interest to define these subtype-specific transcription factors for neurons and to determine how their intersection with pMad/Medea at *wit*-responsive enhancers shapes BMP-dependent neuronal differentiation and synaptic function.

Interestingly, for all previously known BMP-activated genes that include *FMRFa*, *Pburs*, *CCAP*, *Trio*, *Mip* and *Ilp7* (10,11,13), we only found *Pburs* to have conserved *BMP-AE*s within 50kb (Supplementary Table S2). This suggests that other pMad/Medea-responsive motifs play a role in mediating BMP-dependent gene regulation in the VNC. Indeed, a variety of pMad/Medea-responsive motif sequences have been identified in *Drosophila* (27–36), including those outside of the *BMP-AE* or *BMP-SE* consensus, and this diversity is further increased for motifs that bind complexes of activated Smads with other cell type-specific transcription factors and co-factors (105,106). Such diversity would limit the utility of computational discovery approaches to identify those pMad/Medea-responsive *cis*-elements.

Although we did not explicitly demonstrate that the functional *BMP-AE* motifs we identified here are directly bound by pMad/Medea complexes in the CNS, we postulate that this is likely the case. In addition of our *in vitro* and genetic data, two previous studies in the early *Drosophila* embryo and *Drosophila* Kc cells have identified three of the *BMP-AE*s identified here (for *dad13*, *Van34* and *Van36* reporters) to be directly bound by pMad and Medea, using ChIP-seq (36,107). Ongoing studies that aim to confirm that these *BMP-AE*s are indeed directly bound by pMad/Medea complexes and to identify other additional BMP-responsive motifs will expand our understanding of how BMP signaling and pMad/Medea transcriptional activity controls subtype-specific neuronal differentiation and synaptic function.

Towards identification of a directly-regulated BMP effector gene network in neurons

Identification of the direct target genes of developmental signaling pathways is a key step to understanding and modeling the properties of biological systems. Before this study, only *FMRFa* and *trio* have been suggested to be direct targets of BMP-activated Mad transcriptional activity. In addition, a previous microarray study identified 101 genes whose expression is regulated by *wit* in the whole larval CNS (25). Interestingly, comparing the previous microarray analysis of *wit*-responsive genes with the RNA-seq analysis performed here, we found notable differences in the two datasets. Of the 101 genes found in the microarray, only 26 genes were also found to be differentially expressed by RNA-seq analysis here, with 7 of those genes being differentially expressed in the opposite direction (Supplementary Table S3). A potential explanation for this discrepancy could reside in the different sensitivities of these two methodologies, as well as the differences in tissues examined; the microarray analysis used the whole CNS and the ring gland, while our RNA-seq analysis study used VNCs with the brain lobes and ring gland removed. Regardless, these genes represent candidate direct target genes for pMad/Medea transcriptional control, yet leave open the possibility that BMP signaling acts indirectly on many genes, perhaps through the activation or repression of unknown transcription factor intermediaries. Examples of this can be drawn from vertebrate models where BMP4-mediated topographic mapping of trigeminal sensory neurons appear to occur via transcription factor intermediaries (108), and also where retrograde GDNF or NT-3 signaling from target cells induces expression of ETS transcription factors, Pea3 or Er81 respectively, to control appropriate motor and sensory neuronal connectivity (109,110). In such cases, pMad/Medea-dependent direct regulation should be limited to a small number of transcription factors. However, our pairing of *in vivo* reporter analysis and differential transcript profiling identified a large set of *BMP-AE*s and nearby BMP-activated genes; most likely representing genuine regulatory relationships, as demonstrated for *twit*.

We found that *BMP-AEs* embedded in *wit*-responsive fragments were enriched within 20–50 kb of BMP-activated genes. These distances correspond to those found for pMad-bound ChIP peaks enriched within 40 kb of *tkv*-responsive genes in the dorsal ectoderm of 2–3.5 h embryos (36). Also, evidence from large scale enhancer analysis indicates that *Drosophila* enhancers have a bias to regulate the adjacent gene (59), and accordingly we found an enrichment of functional *BMP-AE* motifs adjacent to BMP-activated genes. However, enhancers also operate over longer distances and we do not exclude the likelihood that this is the case for *BMP-AE*s. This may account for the *wit*-responsive activity of 8 genomic fragments whose *BMP-AEs* are not within 50 kb of a BMP-activated gene, but instead within 200 kb of a BMP-activated gene (Supplementary Table S2), which may represent longer distance regulatory relationships.

Amongst the BMP-activated genes near *BMP-AE*s, we found two known regulators of BMP signaling, *dad* and *cv-2*. Loss of function mutants for *dad* display synaptic overgrowth at the NMJ, a role that is consistent with a direct neuronal BMP feedback inhibitor (111). Cv-2 encodes a secreted protein that binds the type I BMP receptor Tkv and heparan sulfate proteoglycans (HSPG) on the cell surface to promote BMP signaling during posterior cross-vein formation in the pupal wing (112,113). The *wit*-responsive expression of this gene in neurons raises the possibility that it plays a BMP signal strength modulatory role at the NMJ. It is intriguing to note that two HSPGs, Syndecan (Sdc) and Dally-like, are both present at the NMJ and influence synaptic growth and active zone form and function, respectively (114). Future studies will shed light on the conservation of molecular mechanisms regulating the binding of the BMP ligands to their receptors between the NMJ and the pupal wing.

A second interesting set of BMP-activated genes are those that control the organization and function of the cytoskeleton. For instance, the *stathmin* gene encodes a tubulin binding phosphoprotein that destabilizes microtubules (115). Stathmin is required for stability and growth of the NMJ, suggesting that Stathmin may also promote the transport of BMP ligands, or other signaling molecules, along the microtubule (116). If this model proves to be correct, it would indicate that BMP signaling directly activates *stathmin* expression in a positive feedback loop.

We identified two additional BMP-activated genes (*cg14274* and *cg7781*) that encode glycosylphosphatidylinositol (GPI) anchored proteins of the Ly-6 family. These genes are of particular interest because of the previous identification of the related *twit* gene as a BMP effector required for the regulation of spontaneous neurotransmit-

ter release at the NMJ (23). All these genes have multiple *BMP-AE*s within broadly expressed *wit*-responsive enhancers near their transcription start sites. This suggests that the transcriptional activation of multiple members of this gene family by BMP signaling is mediated by nearby *BMP-AE*s and that these genes have synergistic, additive or redundant functions to control neurotransmission at the NMJ. It will be interesting to pursue the phenotypic consequences of mutation of this novel family of genes in order to reveal the combined roles of this poorly understood family of proteins in neurotransmission.

DATA AVAILABILITY

The raw sequence data from this study have been submitted to the NCBI GEO under accession number GSE106650.

SUPPLEMENTARY DATA

Supplementary Data are available at NAR Online.

ACKNOWLEDGEMENTS

We are very grateful to Drs Anaïs Bardet and Alexander Stark for performing the motif confidence analysis for the *BMP-AE* motifs in *Drosophila* genomes. We gratefully acknowledge members of the Allan laboratory, Drs Stefan Thor, Pejmun Haghighi and Timothy O'Connor for insightful discussion and critical reading of the manuscript. Also, we thank the anonymous referees whose constructive suggestions greatly improved the manuscript. We are very grateful to Drs T. Michael Underhill and Ryan Vander Werff for assistance with RNA-seq, at the BRC-seq Centre. We are very grateful to Dr Artur Kania for crucial advice and reagents required to perform the chick spinal cord electroporation studies, and to Dr Joy Richman and lab members for infrastructure, lab space and training in chick spinal cord electroporation. We gratefully acknowledge Dr Lyubov Veverytsa (Allan lab) for generating the pStingerattBDsRednls plasmid. We thank Dr Michelle Markstein for providing us the merMer software. We also thank Drs Markus Affolter, Vanessa Auld, Christian Boekel, Justin Kumar, Allen Laughon, Gwenvael Le Dréau, Elisa Marti, Laurel Raftery, Guy Tanentzapf, Esther Verheyen, the Bloomington *Drosophila* Stock Center, the *Drosophila* Genomics Resource Center and P[acman] Resources for fly stocks and molecular reagents.
Author contributions: R.V. and D.W.A. conceived and designed the experiments. R.V. performed most of the experiments. Z.N.K. assisted R.V. with the chick electroporation and processed samples for confocal imaging. T.L. performed the EMSA band shift experiments and generated the wildtype and mutated 8x concatenated *BMP-AE* and *twit* rescue constructs with the help of R.V. G.P. and A.F. initiated this project by establishing collaboration with Alexander Stark to calculate *BMP-AE* motif confidence, and generated the first reporter constructs to analyze BMP-dependent reporter expression in the developing embryo and imaginal discs tissues. S.F. performed the bioinformatics on the RNA-seq data. R.V., T.L., S.F., Z.N.K. and D.W.A. analyzed data. R.V. and D.W.A wrote the paper.

FUNDING

Canadian Institutes of Health Research (CIHR) [MOP-98011, PJT-148905 to D.W.A.]; Deutsche Forschungsgemeinschaft Collaborative Research Centre [SFB592 to G.P.]; Excellence Initiative of the German Federal and State Governments [EXC294 to G.P.]. Funding for open access charge: CIHR [PJT-148905].
Conflict of interest statement. None declared.

REFERENCES

1. Allan,D.W. and Thor,S. (2015) Transcriptional selectors, masters, and combinatorial codes: regulatory principles of neural subtype specification. *Wiley Interdiscip. Rev. Dev. Biol.*, **4**, 505–528.
2. Hobert,O., Carrera,I. and Stefanakis,N. (2010) The molecular and gene regulatory signature of a neuron. *Trends Neurosci.*, **33**, 435–445.
3. Hobert,O. (2011) Regulation of terminal differentiation programs in the nervous system. *Annu. Rev. Cell Dev. Biol.*, **27**, 681–696.
4. Dasen,J.S. (2009) Transcriptional networks in the early development of sensory-motor circuits. *Curr. Top. Dev. Biol.*, **87**, 119–148.
5. da Silva,S. and Wang,F. (2011) Retrograde neural circuit specification by target-derived neurotrophins and growth factors. *Curr. Opin. Neurobiol.*, **21**, 61–67.
6. Hippenmeyer,S., Kramer,I. and Arber,S. (2004) Control of neuronal phenotype: what targets tell the cell bodies. *Trends Neurosci.*, **27**, 482–488.
7. Marqués,G. (2005) Morphogens and synaptogenesis in Drosophila. *J. Neurobiol.*, **64**, 417–434.
8. Layden,M.J., Odden,J.P., Schmid,A., Garces,A., Thor,S. and Doe,C.Q. (2006) Zfh1, a somatic motor neuron transcription factor, regulates axon exit from the CNS. *Dev. Biol.*, **291**, 253–263.
9. Marques,G., Bao,H., Haerry,T.E., Shimell,M.J., Duchek,P., Zhang,B. and O'Connor,M.B. (2002) The Drosophila BMP type II receptor wishful thinking regulates neuromuscular synapse morphology and function. *Neuron*, **33**, 529–543.
10. Allan,D.W., St Pierre,S.E., Miguel-Aliaga,I. and Thor,S. (2003) Specification of neuropeptide cell identity by the integration of retrograde BMP signaling and a combinatorial transcription factor code. *Cell*, **113**, 73–86.
11. Veverytsa,L. and Allan,D.W. (2011) Retrograde BMP signaling controls Drosophila behavior through regulation of a peptide hormone battery. *Development*, **138**, 3147–3157.
12. McCabe,B.D., Marques,G., Haghighi,A.P., Fetter,R.D., Crotty,M.L., Haerry,T.E., Goodman,C.S. and O'Connor,M.B. (2003) The BMP homolog Gbb provides a retrograde signal that regulates synaptic growth at the Drosophila neuromuscular junction. *Neuron*, **39**, 241–254.
13. Miguel-Aliaga,I., Thor,S. and Gould,A.P. (2008) Postmitotic specification of Drosophila insulinergic neurons from pioneer neurons. *PLoS Biol.*, **6**, e58.
14. Aberle,H., Haghighi,A.P., Fetter,R.D., McCabe,B.D., Magalhaes,T.R. and Goodman,C.S. (2002) wishful thinking encodes a BMP type II receptor that regulates synaptic growth in Drosophila. *Neuron*, **33**, 545–558.
15. Goold,C.P. and Davis,G.W. (2007) The BMP ligand Gbb gates the expression of synaptic homeostasis independent of synaptic growth control. *Neuron*, **56**, 109–123.
16. James,R.E., Hoover,K.M., Bulgari,D., McLaughlin,C.N., Wilson,C.G., Wharton,K.A., Levitan,E.S. and Broihier,H.T. (2014) Crimpy enables discrimination of presynaptic and postsynaptic pools of a BMP at the drosophila neuromuscular junction. *Dev. Cell*, **31**, 586–598.
17. Rawson,J.M., Lee,M., Kennedy,E.L. and Selleck,S.B. (2003) Drosophila neuromuscular synapse assembly and function require the TGF-beta type I receptor saxophone and the transcription factor Mad. *J. Neurobiol.*, **55**, 134–150.
18. Rodal,A.A., Blunk,A.D., Akbergenova,Y., Jorquera,R.A., Buhl,L.K. and Littleton,J.T. (2011) A presynaptic endosomal trafficking pathway controls synaptic growth signaling. *J. Cell Biol.*, **193**, 201–217.

19. Vanlandingham,P.A., Fore,T.R., Chastain,L.R., Royer,S.M., Bao,H., Reist,N.E. and Zhang,B. (2013) Epsin 1 promotes synaptic growth by enhancing BMP signal levels in motoneuron nuclei. *PLoS One*, **8**, e65997.
20. Smith,R.B., Machamer,J.B., Kim,N.C., Hays,T.S. and Marques,G. (2012) Relay of retrograde synaptogenic signals through axonal transport of BMP receptors. *J. Cell Sci.*, **125**, 3752–3764.
21. McCabe,B.D., Hom,S., Aberle,H., Fetter,R.D., Marques,G., Haerry,T.E., Wan,H., O'Connor,M.B., Goodman,C.S. and Haghighi,A.P. (2004) Highwire regulates presynaptic BMP signaling essential for synaptic growth. *Neuron*, **41**, 891–905.
22. Berke,B., Wittnam,J., McNeill,E., Van Vactor,D.L. and Keshishian,H. (2013) Retrograde BMP signaling at the synapse: a permissive signal for synapse maturation and activity-dependent plasticity. *J. Neurosci.*, **33**, 17937–17950.
23. Kim,N.C. and Marques,G. (2012) The Ly6 neurotoxin-like molecule target of wit regulates spontaneous neurotransmitter release at the developing neuromuscular junction in Drosophila. *Dev. Neurobiol.*, **72**, 1541–1558.
24. Ball,R.W., Warren-Paquin,M., Tsurudome,K., Liao,E.H., Elazzouzi,F., Cavanagh,C., An,B.S., Wang,T.T., White,J.H. and Haghighi,A.P. (2010) Retrograde BMP signaling controls synaptic growth at the NMJ by regulating trio expression in motor neurons. *Neuron*, **66**, 536–549.
25. Kim,N.C. and Marques,G. (2010) Identification of downstream targets of the bone morphogenetic protein pathway in the Drosophila nervous system. *Dev. Dyn.*, **239**, 2413–2425.
26. Berndt,A.J., Tang,J.C., Ridyard,M.S., Lian,T., Keatings,K. and Allan,D.W. (2015) Gene regulatory mechanisms underlying the spatial and temporal regulation of Target-Dependent gene expression in Drosophila neurons. *PLos Genet.*, **11**, e1005754.
27. Wharton,S.J., Basu,S.P. and Ashe,H.L. (2004) Smad affinity can direct distinct readouts of the embryonic extracellular Dpp gradient in Drosophila. *Curr. Biol.*, **14**, 1550–1558.
28. Walsh,C.M. and Carroll,S.B. (2007) Collaboration between Smads and a Hox protein in target gene repression. *Development*, **134**, 3585–3592.
29. Kim,J., Johnson,K., Chen,H.J., Carroll,S. and Laughon,A. (1997) Drosophila Mad binds to DNA and directly mediates activation of vestigial by Decapentaplegic. *Nature*, **388**, 304–308.
30. Rushlow,C., Colosimo,P.F., Lin,M.C., Xu,M. and Kirov,N. (2001) Transcriptional regulation of the Drosophila gene zen by competing Smad and Brinker inputs. *Genes Dev.*, **15**, 340–351.
31. Xu,X., Yin,Z., Hudson,J.B., Ferguson,E.L. and Frasch,M. (1998) Smad proteins act in combination with synergistic and antagonistic regulators to target Dpp responses to the Drosophila mesoderm. *Genes Dev.*, **12**, 2354–2370.
32. Lin,M.C., Park,J., Kirov,N. and Rushlow,C. (2006) Threshold response of C15 to the Dpp gradient in Drosophila is established by the cumulative effect of Smad and Zen activators and negative cues. *Development*, **133**, 4805–4813.
33. Gao,S., Steffen,J. and Laughon,A. (2005) Dpp-responsive silencers are bound by a trimeric Mad-Medea complex. *J. Biol. Chem.*, **280**, 36158–36164.
34. Weiss,A., Charbonnier,E., Ellertsdottir,E., Tsirigos,A., Wolf,C., Schuh,R., Pyrowolakis,G. and Affolter,M. (2010) A conserved activation element in BMP signaling during Drosophila development. *Nat. Struct. Mol. Biol.*, **17**, 69–76.
35. Pyrowolakis,G., Hartmann,B., Muller,B., Basler,K. and Affolter,M. (2004) A simple molecular complex mediates widespread BMP-induced repression during Drosophila development. *Dev. Cell*, **7**, 229–240.
36. Deignan,L., Pinheiro,M.T., Sutcliffe,C., Saunders,A., Wilcockson,S.G., Zeef,L.A., Donaldson,I.J. and Ashe,H.L. (2016) Regulation of the BMP Signaling-Responsive Transcriptional Network in the Drosophila Embryo. *PLoS Genet.*, **12**, e1006164.
37. Muller,B., Hartmann,B., Pyrowolakis,G., Affolter,M. and Basler,K. (2003) Conversion of an extracellular Dpp/BMP morphogen gradient into an inverse transcriptional gradient. *Cell*, **113**, 221–233.
38. Vuilleumier,R., Springhorn,A., Patterson,L., Koidl,S., Hammerschmidt,M., Affolter,M. and Pyrowolakis,G. (2010) Control of Dpp morphogen signalling by a secreted feedback regulator. *Nat. Cell Biol.*, **12**, 611–617.
39. Esteves,F.F., Springhorn,A., Kague,E., Taylor,E., Pyrowolakis,G., Fisher,S. and Bier,E. (2014) BMPs regulate msx gene expression in the dorsal neuroectoderm of Drosophila and vertebrates by distinct mechanisms. *PLoS Genet.*, **10**, e1004625.
40. Chen,D. and McKearin,D. (2003) Dpp signaling silences bam transcription directly to establish asymmetric divisions of germline stem cells. *Curr. Biol.*, **13**, 1786–1791.
41. Stathopoulos,A. and Levine,M. (2005) Localized repressors delineate the neurogenic ectoderm in the early Drosophila embryo. *Dev. Biol.*, **280**, 482–493.
42. Crocker,J. and Erives,A. (2013) A Schnurri/Mad/Medea complex attenuates the dorsal-twist gradient readout at vnd. *Dev. Biol.*, **378**, 64–72.
43. Stark,A., Lin,M.F., Kheradpour,P., Pedersen,J.S., Parts,L., Carlson,J.W., Crosby,M.A., Rasmussen,M.D., Roy,S., Deoras,A.N. *et al.* (2007) Discovery of functional elements in 12 Drosophila genomes using evolutionary signatures. *Nature*, **450**, 219–232.
44. Kheradpour,P., Stark,A., Roy,S. and Kellis,M. (2007) Reliable prediction of regulator targets using 12 Drosophila genomes. *Genome Res.*, **17**, 1919–1931.
45. Gurdziel,K., Lorberbaum,D.S., Udager,A.M., Song,J.Y., Richards,N., Parker,D.S., Johnson,L.A., Allen,B.L., Barolo,S. and Gumucio,D.L. (2015) Identification and validation of novel Hedgehog-Responsive enhancers predicted by computational analysis of Ci/Gli binding site density. *PLoS One*, **10**, e0145225.
46. Shlyueva,D., Stampfel,G. and Stark,A. (2014) Transcriptional enhancers: from properties to genome-wide predictions. *Nat. Rev. Genet.*, **15**, 272–286.
47. Aerts,S., Quan,X.J., Claeys,A., Sanchez,M.N., Tate,P., Yan,J. and Hassan,B.A. (2010) Robust target gene discovery through transcriptome perturbations and genome-wide enhancer predictions in drosophila uncovers a regulatory basis for sensory specification. *PLoS Biol.*, **8**, e1000435.
48. Markstein,M., Markstein,P., Markstein,V. and Levine,M.S. (2002) Genome-wide analysis of clustered Dorsal binding sites identifies putative target genes in the Drosophila embryo. *Proc. Natl. Acad. Sci. U.S.A.*, **99**, 763–768.
49. Celniker,S.E. and Rubin,G.M. (2003) The Drosophila melanogaster genome. *Annu. Rev. Genomics Hum. Genet.*, **4**, 89–117.
50. Chintapalli,V.R., Wang,J. and Dow,J.A. (2007) Using FlyAtlas to identify better Drosophila melanogaster models of human disease. *Nat. Genet.*, **39**, 715–720.
51. mod,E.C., Roy,S., Ernst,J., Kharchenko,P.V, Kheradpour,P., Negre,N., Eaton,M.L., Landolin,J.M., Bristow,C.A., Ma,L. *et al.* (2010) Identification of functional elements and regulatory circuits by Drosophila modENCODE. *Science*, **330**, 1787–1797.
52. Berger,C., Harzer,H., Burkard,T.R., Steinmann,J., van der Horst,S., Laurenson,A.S., Novatchkova,M., Reichert,H. and Knoblich,J.A. (2012) FACS purification and transcriptome analysis of drosophila neural stem cells reveals a role for Klumpfuss in self-renewal. *Cell Rep.*, **2**, 407–418.
53. Wartlick,O., Mumcu,P., Kicheva,A., Bittig,T., Seum,C., Julicher,F. and Gonzalez-Gaitan,M. (2011) Dynamics of Dpp signaling and proliferation control. *Science*, **331**, 1154–1159.
54. Tsuneizumi,K., Nakayama,T., Kamoshida,Y., Kornberg,T.B., Christian,J.L. and Tabata,T. (1997) Daughters against dpp modulates dpp organizing activity in Drosophila wing development. *Nature*, **389**, 627–631.
55. Haerry,T.E., Khalsa,O., O'Connor,M.B. and Wharton,K.A. (1998) Synergistic signaling by two BMP ligands through the SAX and TKV receptors controls wing growth and patterning in Drosophila. *Development*, **125**, 3977–3987.
56. Osterwalder,T., Yoon,K.S., White,B.H. and Keshishian,H. (2001) A conditional tissue-specific transgene expression system using inducible GAL4. *Proc. Natl. Acad. Sci. U.S.A.*, **98**, 12596–12601.
57. Nagarkar-Jaiswal,S., Lee,P.T., Campbell,M.E., Chen,K., Anguiano-Zarate,S., Gutierrez,M.C., Busby,T., Lin,W.W., He,Y., Schulze,K.L. *et al.* (2015) A library of MiMICs allows tagging of genes and reversible, spatial and temporal knockdown of proteins in Drosophila. *Elife*, **4**, e05338.
58. Hamburger,V. and Hamilton,H.L. (1951) A series of normal stages in the development of the chick embryo. *J. Morphol.*, **88**, 49–92.
59. Kvon,E.Z., Kazmar,T., Stampfel,G., Yanez-Cuna,J.O., Pagani,M., Schernhuber,K., Dickson,B.J. and Stark,A. (2014) Genome-scale

functional characterization of Drosophila developmental enhancers in vivo. *Nature*, **512**, 91–95.
60. Pfeiffer,B.D., Jenett,A., Hammonds,A.S., Ngo,T.T., Misra,S., Murphy,C., Scully,A., Carlson,J.W., Wan,K.H., Laverty,T.R. *et al.* (2008) Tools for neuroanatomy and neurogenetics in Drosophila. *Proc. Natl. Acad. Sci. U.S.A.*, **105**, 9715–9720.
61. Marmion,R.A., Jevtic,M., Springhorn,A., Pyrowolakis,G. and Yakoby,N. (2013) The Drosophila BMPRII, wishful thinking, is required for eggshell patterning. *Dev. Biol.*, **375**, 45–53.
62. Bischof,J., Maeda,R.K., Hediger,M., Karch,F. and Basler,K. (2007) An optimized transgenesis system for Drosophila using germ-line-specific phiC31 integrases. *Proc. Natl. Acad. Sci. U.S.A.*, **104**, 3312–3317.
63. Marx,A., Backes,C., Meese,E., Lenhof,H.P. and Keller,A. (2016) EDISON-WMW: exact dynamic programing solution of the Wilcoxon-Mann-Whitney test. *Genomics Proteomics Bioinforma.*, **14**, 55–61.
64. Uchikawa,M., Ishida,Y., Takemoto,T., Kamachi,Y. and Kondoh,H. (2003) Functional analysis of chicken Sox2 enhancers highlights an array of diverse regulatory elements that are conserved in mammals. *Dev. Cell*, **4**, 509–519.
65. Dobin,A., Davis,C.A., Schlesinger,F., Drenkow,J., Zaleski,C., Jha,S., Batut,P., Chaisson,M. and Gingeras,T.R. (2013) STAR: ultrafast universal RNA-seq aligner. *Bioinformatics*, **29**, 15–21.
66. Pertea,M., Kim,D., Pertea,G.M., Leek,J.T. and Salzberg,S.L. (2016) Transcript-level expression analysis of RNA-seq experiments with HISAT, StringTie and Ballgown. *Nat. Protoc.*, **11**, 1650–1667.
67. Bray,N.L., Pimentel,H., Melsted,P. and Pachter,L. (2016) Near-optimal probabilistic RNA-seq quantification. *Nat. Biotechnol.*, **34**, 525–527.
68. Patro,R., Duggal,G., Love,M.I., Irizarry,R.A. and Kingsford,C. (2017) Salmon provides fast and bias-aware quantification of transcript expression. *Nat. Methods*, **14**, 417–419.
69. Li,B. and Dewey,C.N. (2011) RSEM: accurate transcript quantification from RNA-Seq data with or without a reference genome. *BMC Bioinformatics*, **12**, 323.
70. dos Santos,G., Schroeder,A.J., Goodman,J.L., Strelets,V.B., Crosby,M.A., Thurmond,J., Emmert,D.B., Gelbart,W.M. and FlyBase,C. (2015) FlyBase: introduction of the Drosophila melanogaster Release 6 reference genome assembly and large-scale migration of genome annotations. *Nucleic Acids Res.*, **43**, D690–D697.
71. Love,M.I., Huber,W. and Anders,S. (2014) Moderated estimation of fold change and dispersion for RNA-seq data with DESeq2. *Genome Biol.*, **15**, 550.
72. Robinson,M.D., McCarthy,D.J. and Smyth,G.K. (2010) edgeR: a Bioconductor package for differential expression analysis of digital gene expression data. *Bioinformatics*, **26**, 139–140.
73. Pimentel,H., Bray,N.L., Puente,S., Melsted,P. and Pachter,L. (2017) Differential analysis of RNA-seq incorporating quantification uncertainty. *Nat. Methods*, **14**, 687–690.
74. Grabherr,M.G., Haas,B.J., Yassour,M., Levin,J.Z., Thompson,D.A., Amit,I., Adiconis,X., Fan,L., Raychowdhury,R., Zeng,Q. *et al.* (2011) Full-length transcriptome assembly from RNA-Seq data without a reference genome. *Nat. Biotechnol.*, **29**, 644–652.
75. Wickham,H. (2009) *Ggplot2: Elegant Graphics for Data Analysis*. Springer, NY.
76. Chen,H., Xu,Z., Mei,C., Yu,D. and Small,S. (2012) A system of repressor gradients spatially organizes the boundaries of Bicoid-dependent target genes. *Cell*, **149**, 618–629.
77. R core team (2017) *R: A Language and Environment for Statistical Computing*. R Found. Stat. Comput., Vienna, http://www.R-project.org/.
78. Vacic,V., Iakoucheva,L.M. and Radivojac,P. (2006) Two Sample Logo: a graphical representation of the differences between two sets of sequence alignments. *Bioinformatics*, **22**, 1536–1537.
79. Saka,Y., Hagemann,A.I., Piepenburg,O. and Smith,J.C. (2007) Nuclear accumulation of Smad complexes occurs only after the midblastula transition in Xenopus. *Development*, **134**, 4209–4218.
80. Zhang,X.E., Cui,Z. and Wang,D. (2016) Sensing of biomolecular interactions using fluorescence complementing systems in living cells. *Biosens. Bioelectron.*, **76**, 243–250.
81. Miller,K.E., Kim,Y., Huh,W.K. and Park,H.O. (2015) Bimolecular fluorescence complementation (BiFC) analysis: advances and recent applications for genome-wide interaction studies. *J. Mol. Biol.*, **427**, 2039–2055.
82. Hu,C.D., Chinenov,Y. and Kerppola,T.K. (2002) Visualization of interactions among bZIP and Rel family proteins in living cells using bimolecular fluorescence complementation. *Mol. Cell*, **9**, 789–798.
83. Park,D., Veenstra,J.A., Park,J.H. and Taghert,P.H. (2008) Mapping peptidergic cells in Drosophila: where DIMM fits in. *PLoS One*, **3**, e1896.
84. Landgraf,M. and Thor,S. (2006) Development of Drosophila motoneurons: Specification and morphology. *Semin. Cell Dev. Biol.*, **17**, 3–11.
85. Le Dreau,G., Garcia-Campmany,L., Rabadan,M.A., Ferronha,T., Tozer,S., Briscoe,J. and Marti,E. (2012) Canonical BMP7 activity is required for the generation of discrete neuronal populations in the dorsal spinal cord. *Development*, **139**, 259–268.
86. Le Dréau,G. and Martí,E. (2012) Dorsal-ventral patterning of the neural tube: a tale of three signals. *Dev. Neurobiol.*, **72**, 1471–1481.
87. Karaulanov,E., Knöchel,W. and Niehrs,C. (2004) Transcriptional regulation of BMP4 synexpression in transgenic Xenopus. *EMBO J.*, **23**, 844–856.
88. Osses,N. and Henriquez,J.P. (2014) Bone morphogenetic protein signaling in vertebrate motor neurons and neuromuscular communication. *Front. Cell Neurosci.*, **8**, 453.
89. Chou,H.J., Lai,D.M., Huang,C.W., McLennan,I.S., Wang,H.D. and Wang,P.Y. (2013) BMP4 is a peripherally-derived factor for motor neurons and attenuates glutamate-induced excitotoxicity in vitro. *PLoS One*, **8**, e58441.
90. Zhong,J. and Zou,H. (2014) BMP signaling in axon regeneration. *Curr. Opin. Neurobiol.*, **27**, 127–134.
91. Xiao,L., Michalski,N., Kronander,E., Gjoni,E., Genoud,C., Knott,G. and Schneggenburger,R. (2013) BMP signaling specifies the development of a large and fast CNS synapse. *Nat. Neurosci.*, **16**, 856–864.
92. Sun,M., Thomas,M.J., Herder,R., Bofenkamp,M.L., Selleck,S.B. and O'Connor,M.B. (2007) Presynaptic contributions of chordin to hippocampal plasticity and spatial learning. *J. Neurosci.*, **27**, 7740–7750.
93. Rohrer,H. (2003) The role of bone morphogenetic proteins in sympathetic neuron development. *Drug News Perspect.*, **16**, 589–596.
94. Hegarty,S.V, O'Keeffe,G.W. and Sullivan,A.M. (2013) BMP-Smad 1/5/8 signalling in the development of the nervous system. *Prog. Neurobiol.*, **109**, 28–41.
95. Benveniste,R.J., Thor,S., Thomas,J.B. and Taghert,P.H. (1998) Cell type-specific regulation of the Drosophila FMRF-NH2 neuropeptide gene by Apterous, a LIM homeodomain transcription factor. *Development*, **125**, 4757–4765.
96. Benveniste,R.J. and Taghert,P.H. (1999) Cell type-specific regulatory sequences control expression of the Drosophila FMRF-NH2 neuropeptide gene. *J. Neurobiol.*, **38**, 507–520.
97. Weirauch,M.T. and Hughes,T.R. (2010) Conserved expression without conserved regulatory sequence: the more things change, the more they stay the same. *Trends Genet.*, **26**, 66–74.
98. Ramos,A.I. and Barolo,S. (2013) Low-affinity transcription factor binding sites shape morphogen responses and enhancer evolution. *Philos. Trans. R Soc. L. B Biol. Sci.*, **368**, 20130018.
99. Crocker,J., Noon,E.P. and Stern,D.L. (2016) The soft Touch: Low-Affinity transcription factor binding sites in development and evolution. *Curr. Top. Dev. Biol.*, **117**, 455–469.
100. Howard,M.L. and Davidson,E.H. (2004) cis-Regulatory control circuits in development. *Dev. Biol.*, **271**, 109–118.
101. Yáñez-Cuna,J.O., Kvon,E.Z. and Stark,A. (2013) Deciphering the transcriptional cis-regulatory code. *Trends Genet.*, **29**, 11–22.
102. Spitz,F. and Furlong,E.E.M. (2012) Transcription factors: from enhancer binding to developmental control. *Nat. Rev. Genet.*, **13**, 613–626.
103. Miguel-Aliaga,I., Allan,D.W. and Thor,S. (2004) Independent roles of the dachshund and eyes absent genes in BMP signaling, axon pathfinding and neuronal specification. *Development*, **131**, 5837–5848.
104. Allan,D.W., Park,D., St Pierre,S.E., Taghert,P.H. and Thor,S. (2005) Regulators acting in combinatorial codes also act independently in single differentiating neurons. *Neuron*, **45**, 689–700.
105. Blitz,I.L. and Cho,K.W. (2009) Finding partners: how BMPs select their targets. *Dev. Dyn.*, **238**, 1321–1331.

106. Ross,S. and Hill,C.S. (2008) How the Smads regulate transcription. *Int. J. Biochem. Cell Biol.*, **40**, 383–408.
107. Bortle,K. Van, Peterson,A.J., Takenaka,N., O'Connor,M.B. and Corces,V.G. (2015) CTCF-dependent co-localization of canonical Smad signaling factors at architectural protein binding sites in D. melanogaster. *Cell Cycle*, **14**, 2677–2687.
108. Hodge,L.K., Klassen,M.P., Han,B.X., Yiu,G., Hurrell,J., Howell,A., Rousseau,G., Lemaigre,F., Tessier-Lavigne,M. and Wang,F. (2007) Retrograde BMP signaling regulates trigeminal sensory neuron identities and the formation of precise face maps. *Neuron*, **55**, 572–586.
109. Patel,T.D., Kramer,I., Kucera,J., Niederkofler,V., Jessell,T.M., Arber,S. and Snider,W.D. (2003) Peripheral NT3 signaling is required for ETS protein expression and central patterning of proprioceptive sensory afferents. *Neuron*, **38**, 403–416.
110. Haase,G., Dessaud,E., Garcès,A., De Bovis,B., Birling,M.C., Filippi,P., Schmalbruch,H., Arber,S. and DeLapeyrière,O. (2002) GDNF acts through PEA3 to regulate cell body positioning and muscle innervation of specific motor neuron pools. *Neuron*, **35**, 893–905.
111. Sweeney,S.T. and Davis,G.W. (2002) Unrestricted synaptic growth in spinster-a late endosomal protein implicated in TGF-beta-mediated synaptic growth regulation. *Neuron*, **36**, 403–416.
112. Conley,C.A., Silburn,R., Singer,M.A., Ralston,A., Rohwer-Nutter,D., Olson,D.J., Gelbart,W. and Blair,S.S. (2000) Crossveinless 2 contains cysteine-rich domains and is required for high levels of BMP-like activity during the formation of the cross veins in Drosophila. *Development*, **127**, 3947–3959.
113. Serpe,M., Umulis,D., Ralston,A., Chen,J., Olson,D.J., Avanesov,A., Othmer,H., O'Connor,M.B. and Blair,S.S. (2008) The BMP-binding protein Crossveinless 2 is a short-range, concentration-dependent, biphasic modulator of BMP signaling in Drosophila. *Dev. Cell*, **14**, 940–953.
114. Johnson,K.G., Tenney,A.P., Ghose,A., Duckworth,A.M., Higashi,M.E., Parfitt,K., Marcu,O., Heslip,T.R., Marsh,J.L., Schwarz,T.L. *et al.* (2006) The HSPGs Syndecan and Dallylike bind the receptor phosphatase LAR and exert distinct effects on synaptic development. *Neuron*, **49**, 517–531.
115. Ozon,S., Guichet,A., Gavet,O., Roth,S. and Sobel,A. (2002) Drosophila stathmin: a microtubule-destabilizing factor involved in nervous system formation. *Mol. Biol. Cell*, **13**, 698–710.
116. Graf,E.R., Heerssen,H.M., Wright,C.M., Davis,G.W. and DiAntonio,A. (2011) Stathmin is required for stability of the Drosophila neuromuscular junction. *J. Neurosci.*, **31**, 15026–15034.